J. Fluid Mech. (2023), *vol*. 960, A7, doi:10.1017/jfm.2023.150

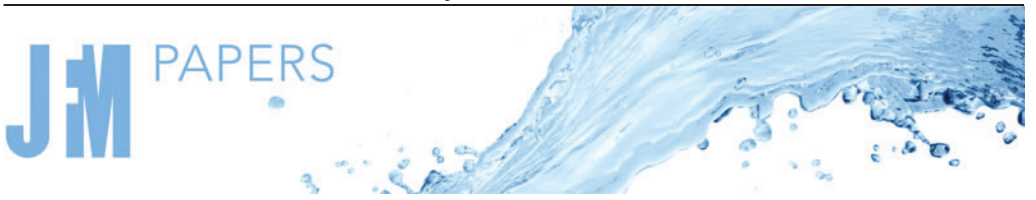

Structure function tensor equations with triple decomposition

Federica Gattere[1], Alessandro Chiarini[1], Emanuele Gallorini[1] and Maurizio Quadrio[1],†

[1]Dipartimento di Scienze e Tecnologie Aerospaziali, Politecnico di Milano, via La Masa 34, 20156 Milano, Italy

(Received 9 September 2022; revised 15 January 2023; accepted 15 February 2023)

Exact budget equations are derived for the coherent and stochastic contributions to the second-order structure function tensor. They extend the anisotropic generalised Kolmogorov equations (AGKE) by considering the coherent and stochastic parts of the Reynolds stress tensor, and are useful for the statistical description of turbulent flows with periodic or quasi-periodic features, like, for example, the alternate shedding after a bluff body. While the original AGKE describe production, transport, inter-component redistribution and dissipation of the Reynolds stresses in the combined space of scales and positions, the new equations, called φAGKE, contain the phase φ as an additional independent variable, and describe the interplay among the mean, coherent and stochastic fields at the various phases. The newly derived φAGKE are then applied to a case where an exactly periodic external forcing drives the flow: a turbulent plane channel flow modified by harmonic spanwise oscillations of the wall to reduce drag. The phase-by-phase action of the oscillating transversal Stokes layer generated by the forcing on the near-wall turbulent structures is observed, and a detailed description of the scale-space interaction among mean, coherent and stochastic fields is provided thanks to the φAGKE.

Key words: turbulent flows

1. Introduction

Understanding the multiscale nature of turbulence and the sustaining mechanisms of turbulent fluctuations is a long-standing effort in fluid mechanics, motivated by the ambition to determine and possibly to manipulate the mean flow. According to the classic arguments by Richardson and Kolmogorov, at large enough Reynolds numbers a clear scale separation is expected between the large energy-containing scales and the small dissipative ones. Fluctuations of different scales interact nonlinearly, and a cascade

† Email address for correspondence: maurizio.quadrio@polimi.it

mechanism transfers energy (on average) towards the dissipating scales. The geometrical information embedded in the larger scales vanishes at smaller ones, so that turbulence becomes locally isotropic below a small enough scale. However, in turbulent flows with practical interest, the scale separation is often incomplete, owing to the finite value of the Reynolds number and to the presence of boundaries; studying such flows is particularly challenging, because of their strongly anisotropic and inhomogeneous nature, which implies that the very concept of scale comes to depend on the position in physical space.

Among the approaches developed over the years to describe anisotropic and inhomogeneous flows, the anisotropic generalised Kolmogorov equations (AGKE) are well suited to account for the multiscale nature of turbulence. The AGKE (Gatti *et al.* 2020) are exact budget equations for each component of the second-order structure function tensor. They extend the generalised Kolmogorov equation (GKE) (see e.g. Danaila *et al.* 2001; Hill 2001), sometimes referred to as the Kármán–Howarth–Monin–Hill equation (Alves Portela, Papadakis & Vassilicos 2017), which, in turn, is the exact budget equation for half the trace of the second-order structure function tensor, i.e. the scale energy. The AGKE, which consider each tensor component separately, describe the production, inter-component redistribution, transport and dissipation of the Reynolds stresses simultaneously across scales and in physical space. Unlike the GKE, they fully account for anisotropy and inhomogeneity, and feature a pressure–strain term that plays a central role in redistribution. Moreover, the AGKE simplify the structural analysis of turbulence, owing to the direct link of each tensor component to the correlation function (Davidson, Nickels & Krogstad 2006; Gatti *et al.* 2020).

The GKE has been already applied to several flows to describe how inhomogeneity changes the Richardson–Kolmogorov scenario, possibly leading to inverse (from small to large scales) energy transfer: the plane channel flow at different Re (Cimarelli, De Angelis & Casciola 2013; Cimarelli *et al.* 2016), the flow over a bump (Mollicone *et al.* 2018), the wake of a square cylinder (Alves Portela *et al.* 2017) and the plane jet Cimarelli *et al.* (2021). Using the GKE, Yao, Mollicone & Papadakis (2022) showed that an intense inverse cascade dominates a boundary layer undergoing bypass transition. Danaila, Voivenel & Varea (2017) derived the variable-viscosity GKE and proved that, in flows with mixing of two or more fluids, all scales evolve in a similar fashion only for regions where viscosity is uniform. Lai, Charonko & Prestridge (2018) derived the variable-density GKE and studied the multi-material effects on the interscale energy transfers in a turbulent round jet, finding that the deformation of smaller turbulent eddies into larger ones accompanies energy transfers. Arun *et al.* (2021) derived the budget equation for the derivative of the two-point velocity correlation for compressible flows, and identified the effects of variable density and dilatation on the energy cascades. The more recent AGKE, instead, have been first demonstrated in a plane channel flow (Gatti *et al.* 2020), and then used to investigate the ascending/descending and direct/inverse cascades of the Reynolds stresses in a turbulent Couette flow (Chiarini *et al.* 2022*b*) and to characterise the structure of turbulence in the flow past a rectangular cylinder (Chiarini *et al.* 2022*a*).

It is not uncommon to encounter turbulent flows in which large scales are relatively organised in space, and follow a temporally repeating pattern. This happens in the presence of an external periodic forcing, or when the flow is quasi-periodic because of instabilities, as in the turbulent wake of bluff bodies. An example of the former class, which is considered in the second half of this paper as a simpler testbench, is the canonical turbulent channel flow modified by periodic spanwise wall oscillation to obtain skin-friction drag reduction (Jung, Mangiavacchi & Akhavan 1992). The spanwise forcing creates a coherent periodic velocity field, known as the generalised Stokes layer (Quadrio & Ricco 2011),

which superimposes on the stochastic turbulent fluctuations. The latter class includes the quasi-periodic Kármán-like vortices in the turbulent wake of bluff bodies, forming after the roll-up of the separating shear layers. Such quasi-periodic structures, usually referred to as coherent motions, interact with the stochastic fluctuations and affect their organisation.

A complete, multiscale description of the interaction among the mean, the coherent (e.g. periodic) and the stochastic fields is highly desirable. Indeed, one can resort to a triple decomposition of the velocity and pressure fields into mean, coherent and stochastic motions, and use it, together with the single-point Reynolds stress budget equations, to describe how these large-scale motions interact with the turbulent fluctuations in physical space. For the spanwise-oscillating wall, Agostini, Touber & Leschziner (2014) found that the phase variation of the stochastic contribution to the Reynolds stresses is mainly driven by production, and that the dissipation plays only a marginal role; they concluded that the increase of the dissipation cannot be the cause of drag reduction. For the alternate shedding behind a bluff body, Kiya & Matsumura (1988) experimentally investigated the various frequency components of the stochastic motions in the wake behind a flat plate perpendicular to the flow. They found that the frequency of the main contributions to the stochastic shear stresses is one-half of the vortex-shedding frequency, explaining it with the different spanwise arrangement of consecutive coherent vortices. In both cases, however, the description was incomplete: a triple decomposition alone does not capture the interaction between coherent and stochastic motions in the space of scales.

Alves Portela, Papadakis & Vassilicos (2020) followed Thiesset, Danaila & Antonia (2014) and used the GKE together with a triple decomposition to describe the interaction between the coherent and stochastic motions in the space of scales and positions. They arrived at two budget equations for the coherent and stochastic parts of the scale energy, and applied them to the turbulent wake past a square cylinder. Interestingly, they found that the mean flow does not feed the stochastic field directly, but it produces kinetic energy that feeds the large-scale coherent structures shed in the wake. Part of this energy is then transferred towards the stochastic turbulent fluctuations, at all scales. Although promising, the approach of Alves Portela *et al.* (2020) is still affected by limitations, discussed by Thiesset & Danaila (2020), that prevent a complete understanding of the interaction among the three fields. This is because their budget equations are obtained by averaging over the phase of the coherent motions, and the phase dependence is lost in the process. Furthermore, being based on the GKE, their procedure considers only the scale energy, and does not describe the pressure–strain redistribution among the various components of the Reynolds stress tensor. Finally, Alves Portela *et al.* (2020) additionally discard directional information by taking orientation averages of every term of the budget equations.

The present work goes one step further to overcome these limitations. We use a triple decomposition to extend the AGKE, and arrive at two phase-by-phase budget equations for the coherent and stochastic parts of each component of the structure function tensor. These equations, named φAGKE, describe the phase-by-phase mean–coherent–stochastic interaction of each component of the Reynolds stresses in the combined space of scales and positions. There is no phase-average involved, so that the description is complete. The paper is structured as follows. After this introduction, in § 2 we briefly recall the AGKE for the classic Reynolds decomposition and introduce the φAGKE for the triple decomposition, discussing the meaning of the various terms. In the second part of the contribution, in § 3, we provide a relatively simple example, and apply the new budget equations to a turbulent channel flow subjected to an oscillatory spanwise wall motion, chosen because of the deterministic nature of the periodic component. In § 4 we demonstrate how the φAGKE describe the mean–coherent–stochastic interaction, and shed light into the complex working mechanism of the oscillating wall. The paper closes with

a brief discussion in § 5. Appendix A contains the detailed derivation of the φAGKE from the Navier–Stokes equations, followed in Appendix B by their specialisation to plane channel flow with oscillating walls. In Appendix C the velocity field induced by the ensemble-averaged quasi-streamwise vortex at different phases is computed and used to support the φAGKE-based analysis of the channel flow with oscillating walls.

2. Mathematical formulation

In this section we introduce the triple decomposition and recall briefly the standard AGKE, before presenting the new φAGKE, the detailed derivation of which is reported in Appendix A.

2.1. *Triple decomposition of the velocity field*

An incompressible turbulent flow, varying in space $\boldsymbol{x}$ and time t, is typically described via its mean and fluctuating velocity and pressure fields, defined after the classic Reynolds decomposition. Provided the flow exhibits well-defined non-stochastic (e.g. periodic) features, the fluctuating field can be further decomposed into a coherent and a stochastic part. Therefore, the velocity field reads

$$\boldsymbol{u} = \boldsymbol{U} + \underbrace{\tilde{\boldsymbol{u}} + \boldsymbol{u}''}_{\boldsymbol{u}'}, \tag{2.1}$$

where $\boldsymbol{U}$, $\boldsymbol{u}'$, $\tilde{\boldsymbol{u}}$ and $\boldsymbol{u}''$ indicate the mean, fluctuating, coherent and stochastic parts of the velocity field $\boldsymbol{u}$. The mean velocity $\boldsymbol{U}$ is defined as $\boldsymbol{U} \equiv \langle \boldsymbol{u} \rangle$, with the operator $\langle \cdot \rangle$ indicating ensemble averaging, which under the ergodic hypothesis becomes equivalent to averaging over homogeneous directions and time (if the flow is statistically stationary). For a single realisation without homogeneous directions, the mean is simply a temporal average:

$$\boldsymbol{U}(\boldsymbol{x}) \equiv \lim_{\tau \to +\infty} \frac{1}{\tau} \int_0^{\tau} \boldsymbol{u}(\boldsymbol{x}, t)\, \mathrm{d}t. \tag{2.2}$$

Considering a periodic motion with period T and phase $\varphi \in (0, 2\pi]$, the overbar $\overline{\cdot}$ denotes the phase average operator over an integer number N of periods. Like $\langle \cdot \rangle$, it includes averaging over the homogeneous directions. Considering again a single realisation without homogeneous directions, $\overline{\cdot}$ is defined as

$$\overline{\boldsymbol{u}}(\boldsymbol{x}, \varphi) \equiv \lim_{N \to +\infty} \frac{1}{N} \sum_{n=0}^{N-1} \boldsymbol{u}\left(\boldsymbol{x}, \left(\frac{\varphi}{2\pi} + n\right) T\right). \tag{2.3}$$

The coherent field $\tilde{\boldsymbol{u}}$ is thus defined as

$$\tilde{\boldsymbol{u}}(\boldsymbol{x}, \varphi) = \overline{\boldsymbol{u}}(\boldsymbol{x}, \varphi) - \boldsymbol{U}(\boldsymbol{x}), \tag{2.4}$$

and the stochastic vector field $\boldsymbol{u}''$ is defined after the triple decomposition (2.1) as $\boldsymbol{u}'' = \boldsymbol{u} - \boldsymbol{U} - \tilde{\boldsymbol{u}}$. An analogous triple decomposition is used to decompose the pressure field $p = P + \tilde{p} + p''$, with $\tilde{p} + p'' = p'$.

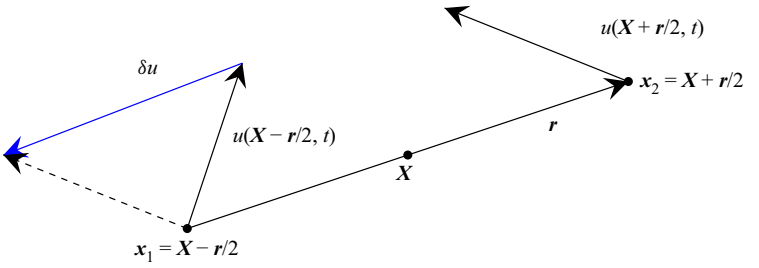

Figure 1. Sketch of two points $\boldsymbol{x}_1$ and $\boldsymbol{x}_2$ involved in the definition of the second-order structure function tensor. Here, $\boldsymbol{X}=(\boldsymbol{x}_1+\boldsymbol{x}_2)/2$ and $\boldsymbol{r}=\boldsymbol{x}_2-\boldsymbol{x}_1$ indicate their mid-point and separation vector, respectively, and $\delta\boldsymbol{u}=\boldsymbol{u}_2-\boldsymbol{u}_1$ is the velocity increment between the two points.

2.2. *The AGKE*

Before presenting the φAGKE, the standard AGKE based on the Reynolds decomposition are recalled. Full details of their derivation from the incompressible Navier–Stokes equations are provided by Gatti *et al.* (2020).

Exact budget equations can be written for the components of the second-order structure function tensor $\langle\delta u_i\delta u_j\rangle$, where $\delta u_i=u_i(\boldsymbol{X}+\boldsymbol{r}/2,\,t)-u_i(\boldsymbol{X}-\boldsymbol{r}/2,\,t)$ is the ith component of the velocity difference between two points $\boldsymbol{x}_1$ and $\boldsymbol{x}_2$, identified by their midpoint $\boldsymbol{X}=(\boldsymbol{x}_1+\boldsymbol{x}_2)/2$ and their separation vector $\boldsymbol{r}=(\boldsymbol{x}_2-\boldsymbol{x}_1)$, as shown by the sketch in figure 1. The Reynolds decomposition leads to budget equations for $\delta U_i\delta U_j$ and $\langle\delta u_i'\delta u_j'\rangle$. In general, the time-independent tensor $\delta U_i\delta U_j$ depends upon six independent variables, i.e. the six coordinates of $\boldsymbol{X}$ and $\boldsymbol{r}$. The tensor $\langle\delta u_i'\delta u_j'\rangle$ additionally features time t as an independent variable if the process is not statistically stationary (e.g. periodic), and is related to the Reynolds stresses $\langle u_i'u_j'\rangle$ and to the spatial correlation tensor R_{ij} (Davidson *et al.* 2006; Agostini & Leschziner 2017) as

$$\langle\delta u_i'\delta u_j'\rangle(\boldsymbol{X},\boldsymbol{r},t)=V_{ij}(\boldsymbol{X},\boldsymbol{r},t)-R_{ij}(\boldsymbol{X},\boldsymbol{r},t)-R_{ij}(\boldsymbol{X},-\boldsymbol{r},t),\tag{2.5}$$

where

$$V_{ij}(\boldsymbol{X},\boldsymbol{r},t)=\langle u_i'u_j'\rangle\left(\boldsymbol{X}+\frac{\boldsymbol{r}}{2},t\right)+\langle u_i'u_j'\rangle\left(\boldsymbol{X}-\frac{\boldsymbol{r}}{2},t\right)\tag{2.6}$$

is the sum of the single-point Reynolds stresses evaluated at the two points $\boldsymbol{X}\pm\boldsymbol{r}/2$ and

$$R_{ij}(\boldsymbol{X},\boldsymbol{r},t)=\left\langle u_i'\left(\boldsymbol{X}+\frac{\boldsymbol{r}}{2},t\right)u_j'\left(\boldsymbol{X}-\frac{\boldsymbol{r}}{2},t\right)\right\rangle\tag{2.7}$$

is the two-point spatial correlation function.

The budget equations for the components of the mean second-order structure function tensor $\delta U_i\delta U_j$ are presented here for the first time; they were not reported by Gatti *et al.* (2020), and the tensor has received little attention so far, owing to its irrelevance in homogeneous isotropic turbulence, where there is no mean flow. The mean AGKE are written compactly as

$$\frac{\partial\Phi_{k,ij}^m}{\partial r_k}+\frac{\partial\Psi_{k,ij}^m}{\partial X_k}=\Xi_{ij}^m,\tag{2.8}$$

where the repeated index k implies summation. The following notation is adopted. Uppercase letters (e.g. Φ, Ψ and Ξ) are used to denote time-averaged quantities and

lowercase letters (e.g. ϕ, ψ and ξ) are used for phase-dependent quantities. Furthermore, superscripts m, f, c and s are used to label terms in the budget equations for the mean structure function tensor $\delta U_i \delta U_j$, the fluctuating structure function tensor $\langle \delta u_i' \delta u_j' \rangle$, the coherent structure function tensor $\overline{\delta \tilde{u}_i \delta \tilde{u}_j} = \delta \tilde{u}_i \delta \tilde{u}_j$ and the stochastic structure function tensor $\overline{\delta u_i'' \delta u_j''}$.

The fluxes $\Phi^m_{k,ij}$ and $\Psi^m_{k,ij}$ are the mean scale- and physical-space fluxes, i.e.

$$\Phi^m_{k,ij} = \underbrace{\delta U_k \delta U_i \delta U_j}_{\text{Mean transport}} + \underbrace{\delta U_j \langle \delta u_k' \delta u_i' \rangle + \delta U_i \langle \delta u_k' \delta u_j' \rangle}_{\text{Fluctuating transport}} \underbrace{-2\nu \frac{\partial \delta U_i \delta U_j}{\partial r_k}}_{\text{Viscous diffusion}} \quad k = 1, 2, 3 \tag{2.9}$$

and

$$\Psi^m_{k,ij} = \underbrace{U_k^* \delta U_i \delta U_j}_{\text{Mean transport}} + \underbrace{\delta U_j \langle u_k'^* \delta u_i' \rangle + \delta U_i \langle u_k'^* \delta u_j' \rangle}_{\text{Fluctuating transport}} \underbrace{+\frac{1}{\rho} \delta P \delta U_j \delta_{ki} + \frac{1}{\rho} \delta P \delta U_i \delta_{kj}}_{\text{Pressure transport}}$$
$$\underbrace{-\frac{\nu}{2} \frac{\partial \delta U_i \delta U_j}{\partial X_k}}_{\text{Viscous diffusion}} \quad k = 1, 2, 3, \tag{2.10}$$

where δ_{ij} is the Kronecker delta, ν is the kinematic viscosity and the asterisk superscript $(\cdot)^*$ indicates the arithmetic average of a quantity between the two points $\boldsymbol{X} \pm \boldsymbol{r}/2$. The term Ξ^m_{ij}, instead, is the mean source and reads

$$\Xi^m_{ij} = \underbrace{-\left[-\langle u_k'^* \delta u_j' \rangle \delta \left(\frac{\partial U_i}{\partial x_k} \right) - \langle u_k'^* \delta u_i' \rangle \delta \left(\frac{\partial U_j}{\partial x_k} \right) - \langle \delta u_k' \delta u_j' \rangle \left(\frac{\partial U_i}{\partial x_k} \right)^* - \langle \delta u_k' \delta u_i' \rangle \left(\frac{\partial U_j}{\partial x_k} \right)^* \right]}_{\text{Mean-fluctuating production } (P^{mf}_{ij})}$$
$$\underbrace{+\frac{1}{\rho} \delta P \frac{\partial \delta U_i}{\partial X_j} + \frac{1}{\rho} \delta P \frac{\partial \delta U_j}{\partial X_i}}_{\text{Pressure strain } (\Pi^m_{ij})} \underbrace{-4\epsilon^{m*}_{ij}}_{\text{Dissipation } (D^m_{ij})} + \underbrace{\delta U_j \delta F_i + \delta U_i \delta F_j}_{\text{Forcing interaction } (F^m_{ij})}. \tag{2.11}$$

The standard AGKE, presented by Gatti *et al.* (2020), pertain to increments of the fluctuating velocity field, and describe the production, transport, redistribution and dissipation of each component, in physical space $\boldsymbol{X}$ and in the space of scales $\boldsymbol{r}$. They can be written compactly as

$$\frac{\partial \langle \delta u_i' \delta u_j' \rangle}{\partial t} + \frac{\partial \Phi^f_{k,ij}}{\partial r_k} + \frac{\partial \Psi^f_{k,ij}}{\partial X_k} = \Xi^f_{ij}. \tag{2.12}$$

The scale-space fluxes $\Phi^f_{k,ij}$ and physical-space fluxes $\Psi^f_{k,ij}$ are defined as

$$\Phi^f_{k,ij} = \underbrace{\langle \delta U_k \delta u_i' \delta u_j' \rangle}_{\text{Mean transport}} + \underbrace{\langle \delta u_k' \delta u_i' \delta u_j' \rangle}_{\text{Fluctuating transport}} \underbrace{-2\nu \frac{\partial}{\partial r_k} \langle \delta u_i' \delta u_j' \rangle}_{\text{Viscous diffusion}} \quad k = 1, 2, 3 \tag{2.13}$$

and

$$\Psi^f_{k,ij} = \underbrace{\langle U^*_k \delta u'_i \delta u'_j \rangle}_{\text{Mean transport}} + \underbrace{\langle u'^*_k \delta u'_i \delta u'_j \rangle}_{\text{Fluctuating transport}} + \underbrace{\frac{1}{\rho}\langle \delta p' \delta u'_i \rangle \delta_{kj} + \frac{1}{\rho}\langle \delta p' \delta u'_j \rangle \delta_{ki}}_{\text{Pressure transport}}$$
$$\underbrace{-\frac{\nu}{2}\frac{\partial}{\partial X_k}\langle \delta u'_i \delta u'_j \rangle}_{\text{Viscous diffusion}} \quad k = 1, 2, 3. \tag{2.14}$$

The term Ξ^f_{ij} in (2.12) is the source for $\langle \delta u'_i \delta u'_j \rangle$ and reads

$$\Xi^f_{ij} = \underbrace{-\langle u'^*_k \delta u'_j \rangle \delta \left(\frac{\partial U_i}{\partial x_k}\right) - \langle u'^*_k \delta u'_i \rangle \delta \left(\frac{\partial U_j}{\partial x_k}\right) - \langle \delta u'_k \delta u'_j \rangle \left(\frac{\partial U_i}{\partial x_k}\right)^* - \langle \delta u'_k \delta u'_i \rangle \left(\frac{\partial U_j}{\partial x_k}\right)^*}_{\text{Mean-fluctuating production } (P^{mf}_{ij})}$$
$$+ \underbrace{\frac{1}{\rho}\left\langle \delta p' \frac{\partial \delta u'_i}{\partial X_j}\right\rangle + \frac{1}{\rho}\left\langle \delta p' \frac{\partial \delta u'_j}{\partial X_i}\right\rangle}_{\text{Pressure strain } (\Pi^f_{ij})} \underbrace{-4\epsilon^{f*}_{ij}}_{\text{Dissipation } (D^f_{ij})} + \underbrace{\langle \delta u'_j \delta f'_i \rangle + \langle \delta u'_i \delta f'_j \rangle}_{\text{Forcing interaction } (F^f_{ij})}, \tag{2.15}$$

in which ϵ^f_{ij} is the pseudo-dissipation tensor $\langle \partial u'_i/\partial x_k \partial u'_j/\partial x_k \rangle$. The source term Ξ^f_{ij} identifies scales and positions with a net sink ($\Xi^f_{ij} < 0$) or a net source ($\Xi^f_{ij} > 0$) for each component of the Reynolds stresses. The separation of Ξ^f_{ij} into its constituent terms provides insight into mean-fluctuating production P^{mf}_{ij} (which also appears in (2.11) with opposite sign), redistribution Π^f_{ij}, dissipation D^f_{ij} and interaction with external fluctuating volume forces F^f_{ij} of turbulent stresses among scales and positions (note that the forcing interaction term was missing in the original AGKE formulated by Gatti *et al.* (2020)). The flux vectors describe the various transfer processes, and their field lines visualise how fluctuations are transferred among scales and positions, via direct and inverse cascades. It should be recalled that, as stressed by Gatti *et al.* (2020), when interpreting AGKE results to extract structural turbulence information, local peaks of the structure functions always need to be connected to local maxima/minima of the correlation functions whenever a separation along an inhomogeneous direction is involved.

2.3. *The phase-aware AGKE (φAGKE)*

By using the triple decomposition (2.1), the phase-averaged fluctuating structure function tensor $\overline{\delta u'_i \delta u'_j}(\boldsymbol{X}, \boldsymbol{r}, \varphi)$ can be separated into its coherent and stochastic parts, i.e.

$$\overline{\delta u'_i \delta u'_j}(\boldsymbol{X}, \boldsymbol{r}, \varphi) = \overline{\delta \tilde{u}_i \delta \tilde{u}_j}(\boldsymbol{X}, \boldsymbol{r}, \varphi) + \overline{\delta u''_i \delta u''_j}(\boldsymbol{X}, \boldsymbol{r}, \varphi); \tag{2.16}$$

note that $\overline{\delta \tilde{u}_i \delta \tilde{u}_j} \equiv \delta \tilde{u}_i \delta \tilde{u}_j$ owing to the definition of the phase-average operator. Two budget equations, called φAGKE, can be written for $\delta \tilde{u}_i \delta \tilde{u}_j$ and $\overline{\delta u''_i \delta u''_j}$, which include, unlike the standard AGKE, the interplay among the mean, coherent and stochastic fields at each phase φ. These new equations extend in a significant way the work of Thiesset *et al.* (2014)

and Alves Portela *et al.* (2020), which considered the budget equations for $\langle \delta\tilde{u}_i \delta\tilde{u}_i \rangle (\boldsymbol{X}, \boldsymbol{r})$ and $\langle \delta u_i'' \delta u_i'' \rangle (\boldsymbol{X}, \boldsymbol{r})$. They applied the triple decomposition to the trace $\langle \delta u_i' \delta u_i' \rangle$ of the second-order structure function tensor, instead of considering the whole tensor. The major difference, though, is that the dependence on the phase φ of the coherent motion (or external forcing) was lost, because of the use of the $\langle \cdot \rangle$ operator. On the contrary, the φAGKE retain full phase information.

The step-by-step derivation of the φAGKE from the incompressible Navier–Stokes equations is described in Appendix A. At each phase φ, they link the phase variation of each component of the coherent and stochastic structure function tensors, at a given scale $\boldsymbol{r}$ and position $\boldsymbol{X}$, to the unbalance among inter-component redistribution, scale-space transport, dissipation and mean–coherent–stochastic interaction. The last term is obviously absent in the classic AGKE.

The equations for the coherent and stochastic parts can be compactly written as

$$\frac{2\pi}{T}\frac{\partial \delta\tilde{u}_i \delta\tilde{u}_j}{\partial \varphi} + \frac{\partial \phi^c_{k,ij}}{\partial r_k} + \frac{\partial \psi^c_{k,ij}}{\partial X_k} = \xi^c_{ij} + \zeta^c_{ij} \tag{2.17}$$

and

$$\frac{2\pi}{T}\frac{\partial \overline{\delta u_i'' \delta u_j''}}{\partial \varphi} + \frac{\partial \phi^s_{k,ij}}{\partial r_k} + \frac{\partial \psi^s_{k,ij}}{\partial X_k} = \xi^s_{ij}, \tag{2.18}$$

where, as above, the repeated index k implies summation.

The first term in each of (2.17) and (2.18) represents the phase variation of the coherent and stochastic components of the structure function tensor. The coherent and stochastic scale fluxes $\phi^c_{k,ij}$ and $\phi^s_{k,ij}$, i.e. the fluxes of $\delta\tilde{u}_i\delta\tilde{u}_j$ and $\overline{\delta u_i'' \delta u_j''}$ in the space of scales, are defined as

$$\phi^c_{k,ij} = \underbrace{\delta U_k \delta\tilde{u}_i \delta\tilde{u}_j}_{\text{Mean transport}} + \underbrace{\delta\tilde{u}_k \delta\tilde{u}_i \delta\tilde{u}_j}_{\text{Coherent transport}} + \underbrace{\overline{\delta u_k'' \delta u_i''}\,\delta\tilde{u}_j + \overline{\delta u_k'' \delta u_j''}\,\delta\tilde{u}_i}_{\text{Stochastic transport}} \underbrace{-2\nu \frac{\partial \delta\tilde{u}_i \delta\tilde{u}_j}{\partial r_k}}_{\text{Viscous diffusion}} \quad k = 1, 2, 3 \tag{2.19}$$

and

$$\phi^s_{k,ij} = \underbrace{\delta U_k \overline{\delta u_i'' \delta u_j''}}_{\text{Mean transport}} + \underbrace{\delta\tilde{u}_k \overline{\delta u_i'' \delta u_j''}}_{\text{Coherent transport}} + \underbrace{\overline{\delta u_k'' \delta u_i'' \delta u_j''}}_{\text{Stochastic transport}} \underbrace{-2\nu \frac{\partial \overline{\delta u_i'' \delta u_j''}}{\partial r_k}}_{\text{Viscous diffusion}} \quad k = 1, 2, 3. \tag{2.20}$$

The coherent and stochastic spatial flux terms $\psi^c_{k,ij}$ and $\psi^s_{k,ij}$, i.e. the fluxes of $\delta\tilde{u}_i\delta\tilde{u}_j$ and $\overline{\delta u_i'' \delta u_j''}$ in physical space, are defined as

$$\psi^c_{k,ij} = \underbrace{U^*_k \delta\tilde{u}_i \delta\tilde{u}_j}_{\text{Mean transport}} + \underbrace{\tilde{u}^*_k \delta\tilde{u}_i \delta\tilde{u}_j}_{\text{Coherent transport}} + \underbrace{\overline{u_k''^* \delta u_i''}\,\delta\tilde{u}_j + \overline{u_k''^* \delta u_j''}\,\delta\tilde{u}_i}_{\text{Stochastic transport}} + \underbrace{\frac{1}{\rho}\delta\tilde{p}\delta\tilde{u}_i\delta_{kj}}_{\text{Pressure transport}}$$
$$\underbrace{+\frac{1}{\rho}\delta\tilde{p}\delta\tilde{u}_j\delta_{ki}}_{\text{Pressure transport}} \underbrace{-\frac{\nu}{2}\frac{\partial \delta\tilde{u}_i\delta\tilde{u}_j}{\partial X_k}}_{\text{Viscous diffusion}} \quad k = 1, 2, 3, \tag{2.21}$$

$$\psi^s_{k,ij} = \underbrace{U^*_k\overline{\delta u''_i \delta u''_j}}_{\text{Mean transport}} + \underbrace{\tilde{u}^*_k\overline{\delta u''_i \delta u''_j}}_{\text{Coherent transport}} + \underbrace{\overline{u''^*_k \delta u''_i \delta u''_j}}_{\text{Stochastic transport}} + \underbrace{\frac{1}{\rho}\overline{\delta p'' \delta u''_i}\delta_{kj} + \frac{1}{\rho}\overline{\delta p'' \delta u''_j}\delta_{ki}}_{\text{Pressure transport}}$$

$$\underbrace{-\frac{\nu}{2}\frac{\partial \overline{\delta u''_i \delta u''_j}}{\partial X_k}}_{\text{Viscous diffusion}} \quad k = 1, 2, 3. \tag{2.22}$$

The differences with the fluxes (2.13) and (2.14) appearing in the standard AGKE are worth noticing. Two new terms appear here to account for the effect of the coherent field upon transport in the stochastic field, labelled as coherent transport in (2.20) and (2.22). Vice versa, how the stochastic field affects transport in the coherent field is reflected by the stochastic transport term in (2.19) and (2.21).

The coherent and stochastic source terms ξ^c_{ij} and ξ^s_{ij} denote the scale-space net production of $\delta\tilde{u}_i\delta\tilde{u}_j$ and $\overline{\delta u''_i \delta u''_j}$. They can be either positive or negative, and read

$$\xi^c_{ij} = \underbrace{-\delta\tilde{u}_j\delta\tilde{u}_k\left(\frac{\partial U_i}{\partial x_k}\right)^* - \delta\tilde{u}_i\delta\tilde{u}_k\left(\frac{\partial U_j}{\partial x_k}\right)^* - \delta\tilde{u}_j\tilde{u}^*_k\delta\left(\frac{\partial U_i}{\partial x_k}\right) - \delta\tilde{u}_i\tilde{u}^*_k\delta\left(\frac{\partial U_j}{\partial x_k}\right)}_{\text{Mean–coherent production } (p^{mc}_{ij})}$$

$$\underbrace{-\left[-\overline{\delta u''_j \delta u''_k}\left(\frac{\partial \tilde{u}_i}{\partial x_k}\right)^* - \overline{\delta u''_i \delta u''_k}\left(\frac{\partial \tilde{u}_j}{\partial x_k}\right)^* - \overline{\delta u''_j u''^*_k}\delta\left(\frac{\partial \tilde{u}_i}{\partial x_k}\right) - \overline{\delta u''_i u''^*_k}\delta\left(\frac{\partial \tilde{u}_j}{\partial x_k}\right)\right]}_{\text{Coherent–stochastic production } (p^{cs}_{ij})}$$

$$\underbrace{+\frac{1}{\rho}\delta\tilde{p}\frac{\partial\delta\tilde{u}_i}{\partial X_j} + \frac{1}{\rho}\delta\tilde{p}\frac{\partial\delta\tilde{u}_j}{\partial X_i}}_{\text{Pressure strain } (\pi^c_{ij})} \underbrace{-4\epsilon^{c*}_{ij}}_{\text{Dissipation}(d^c_{ij})} + \underbrace{\delta\tilde{u}_j\delta\tilde{f}_i + \delta\tilde{u}_i\delta\tilde{f}_j}_{\text{Forcing interaction}(f^c_{ij})}, \tag{2.23}$$

$$\xi^s_{ij} = \underbrace{-\overline{\delta u''_j \delta u''_k}\left(\frac{\partial U_i}{\partial x_k}\right)^* - \overline{\delta u''_i \delta u''_k}\left(\frac{\partial U_j}{\partial x_k}\right)^* - \overline{\delta u''_j u''^*_k}\delta\left(\frac{\partial U_i}{\partial x_k}\right) - \overline{\delta u''_i u''^*_k}\delta\left(\frac{\partial U_j}{\partial x_k}\right)}_{\text{Mean–stochastic production}(p^{ms}_{ij})}$$

$$\underbrace{+\left[-\overline{\delta u''_j \delta u''_k}\left(\frac{\partial \tilde{u}_i}{\partial x_k}\right)^* - \overline{\delta u''_i \delta u''_k}\left(\frac{\partial \tilde{u}_j}{\partial x_k}\right)^* - \overline{\delta u''_j u''^*_k}\delta\left(\frac{\partial \tilde{u}_i}{\partial x_k}\right) - \overline{\delta u''_i u''^*_k}\delta\left(\frac{\partial \tilde{u}_j}{\partial x_k}\right)\right]}_{\text{Coherent–stochastic production } (p^{cs}_{ij})}$$

$$\underbrace{+\frac{1}{\rho}\overline{\delta p''\frac{\partial\delta u''_i}{\partial X_j}} + \frac{1}{\rho}\overline{\delta p''\frac{\partial\delta u''_j}{\partial X_i}}}_{\text{Pressure strain } (\pi^s_{ij})} \underbrace{-4\epsilon^{s*}_{ij}}_{\text{Dissipation}(d^s_{ij})} + \underbrace{\overline{\delta u''_j \delta f''_i} + \overline{\delta u''_i \delta f''_j}}_{\text{Forcing interaction}(f^s_{ij})}. \tag{2.24}$$

Among the terms appearing in the source, the mean–coherent and mean–stochastic productions p^{mc}_{ij} and p^{ms}_{ij} indicate the scales and positions where the mean flow feeds, or drains energy from, the coherent and stochastic fields: they are not positive definite, and therefore can be either sources or sinks. They both contribute to the mean-fluctuating production P^{mf}_{ij} in (2.11), as $P^{mf}_{ij} = \langle p^{mc}_{ij}\rangle + \langle p^{ms}_{ij}\rangle$. The coherent–stochastic production p^{cs}_{ij} indicates the exchange of stresses between the coherent and stochastic fields, and

appears in the budgets for $\delta\tilde{u}_i\delta\tilde{u}_j$ and $\overline{\delta u_i''\delta u_j''}$ with opposite sign. Terms d_{ij}^c and d_{ij}^s denote viscous dissipation, and the pressure–strain terms π_{ij}^c and π_{ij}^s describe the interplay between pressure and velocity fields. Pressure–strain terms involve neither production nor dissipation of energy, and no cross-talk between coherent and fluctuating fields. Overall, among the source terms, the productions p_{ij}^{mc}, p_{ij}^{ms} and p_{ij}^{cs} are the only ones that connect the mean, coherent and fluctuating budgets, and are essential to ascertain how the mean, stochastic and coherent fields force each other. The forcing interactions f_{ij}^c and f_{ij}^s represent the power injected into the system by the interaction of a coherent and stochastic external volume forcing with the coherent and stochastic flow fields, respectively. Finally, in (2.17) for $\delta\tilde{u}_i\delta\tilde{u}_j$ a new term ζ_{ij}^c appears on the right-hand side. It describes the inter-phase interaction driven by the coherent flow field, and is defined as

$$\begin{aligned}\zeta_{ij}^c = &\frac{\partial}{\partial r_k}\left[\langle\delta\tilde{u}_i\delta\tilde{u}_k\rangle\,\delta\tilde{u}_j + \langle\delta\tilde{u}_j\delta\tilde{u}_k\rangle\,\delta\tilde{u}_i\right] + \frac{\partial}{\partial X_k}\left[\langle\tilde{u}_k^*\delta\tilde{u}_i\rangle\,\delta\tilde{u}_j + \langle\tilde{u}_k^*\delta\tilde{u}_j\rangle\,\delta\tilde{u}_i\right]\\
&+\frac{\partial}{\partial r_k}\left[\langle\delta u_i''\delta u_k''\rangle\,\delta\tilde{u}_j + \langle\delta u_j''\delta u_k''\rangle\delta\tilde{u}_i\right] + \frac{\partial}{\partial X_k}\left[\langle u_k''^*\delta u_i''\rangle\,\delta\tilde{u}_j + \langle u_k''^*\delta u_j''\rangle\delta\tilde{u}_i\right]\\
&-\langle\delta\tilde{u}_i\delta\tilde{u}_k\rangle\left(\frac{\partial\tilde{u}_j}{\partial x_k}\right)^* - \langle\delta\tilde{u}_j\delta\tilde{u}_k\rangle\left(\frac{\partial\tilde{u}_i}{\partial x_k}\right)^* - \langle\delta\tilde{u}_i\tilde{u}_k^*\rangle\,\delta\left(\frac{\partial\tilde{u}_j}{\partial x_k}\right) - \langle\delta\tilde{u}_j\tilde{u}_k^*\rangle\,\delta\left(\frac{\partial\tilde{u}_i}{\partial x_k}\right)\\
&-\langle\delta u_i''\delta u_k''\rangle\left(\frac{\partial\tilde{u}_j}{\partial x_k}\right)^* - \langle\delta u_j''\delta u_k''\rangle\left(\frac{\partial\tilde{u}_i}{\partial x_k}\right)^* - \langle\delta u_i''u_k''^*\rangle\,\delta\left(\frac{\partial\tilde{u}_j}{\partial x_k}\right) - \langle\delta u_j''u_k''^*\rangle\delta\left(\frac{\partial\tilde{u}_i}{\partial x_k}\right).\end{aligned} \tag{2.25}$$

The terms in the last two rows above resemble a production term, and indicate the production of $\delta\tilde{u}_i\delta\tilde{u}_j$ due to the correlation of each phase with all the others.

By averaging equations (2.17) and (2.18) over the phases, the budget equations for $\langle\delta\tilde{u}_i\delta\tilde{u}_j\rangle(\boldsymbol{X},\boldsymbol{r})$ and $\langle\delta u_i''\delta u_j''\rangle(\boldsymbol{X},\boldsymbol{r})$ are obtained. In doing this, the inter-phase contributions vanish, since by definition they have zero average. The sum of the equations for the three diagonal components of $\langle\delta\tilde{u}_i\delta\tilde{u}_j\rangle$ and $\langle\delta u_i''\delta u_j''\rangle$ yields the GKE used by Alves Portela *et al.* (2020). If the equations for $\langle\delta\tilde{u}_i\delta\tilde{u}_j\rangle$ and $\langle\delta u_i''\delta u_j''\rangle$ are added together, the standard AGKE for the fluctuating field $\langle\delta u_i'\delta u_j'\rangle$ are recovered.

3. Turbulent drag reduction by a spanwise-oscillating wall

The φAGKE are now applied to a fully developed turbulent channel flow subjected to a spanwise harmonic oscillation of the walls. This flow is a convenient example where the deterministic external periodic forcing provides an unambiguous definition of the phase, yet the physics behind drag reduction is interesting and not fully understood yet.

The spanwise oscillating wall is a well-known skin-friction drag reduction technique, intensely studied over the last thirty years (see Ricco, Skote & Leschziner 2021, and references therein). The channel walls periodically move along the spanwise direction, according to

$$w_w(t) = A\sin\left(\frac{2\pi}{T}t\right), \tag{3.1}$$

where A and T are the prescribed amplitude and period of the sinusoidal oscillation and w_w is the spanwise velocity of the wall. Here, x, y and z (u, v and w) denote the streamwise,

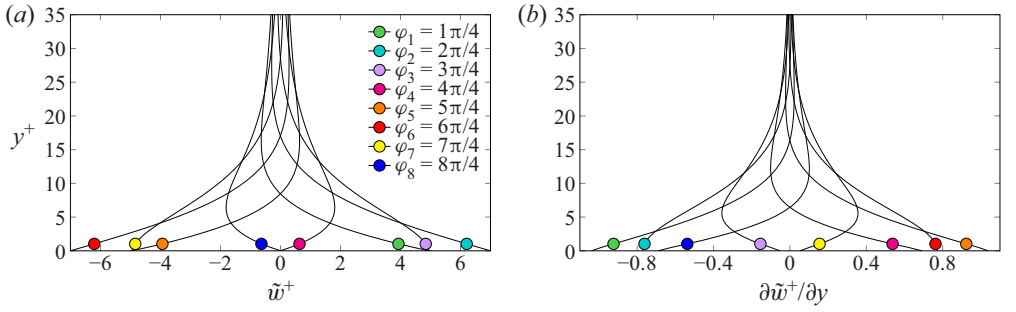

Figure 2. Wall-normal profile of the spanwise coherent velocity $\tilde{w}^+$ (*a*) and shear $\partial\tilde{w}^+/\partial y$ (*b*), plotted at eight equally spaced phases $\varphi_1, \ldots, \varphi_8$ along the period $T^+ = 250$.

wall-normal and spanwise directions (velocity components); the alternative notation $x_1 = x$ ($u_1 = u$), $x_2 = y$ ($u_2 = v$) and $x_3 = z$ ($u_3 = w$) is also used. The harmonic oscillation generates a periodic (coherent) spanwise cross-flow, which even for a turbulent streamwise flow is well described (Quadrio & Sibilla 2000) by the analytical laminar solution of the second Stokes problem, usually referred to as the Stokes layer:

$$w(y, \varphi) = A \exp\left(-\sqrt{\frac{\omega}{2\nu}}y\right) \sin\left(\varphi - \sqrt{\frac{\omega}{2\nu}}y\right), \tag{3.2}$$

where φ is the phase of the oscillation and $\omega = 2\pi/T$. Figure 2 shows the coherent spanwise velocity field (the Stokes layer) generated by the harmonic oscillations, and its derivative in the wall-normal direction (the Stokes shear): the oscillating period is subdivided into eight equally spaced phases $\varphi_1, \varphi_2, \ldots, \varphi_8$, where $\varphi_i = i\pi/4$. From here on, a $+$ superscript is used to indicate quantities made dimensionless with the friction velocity $u_\tau = \sqrt{\tau_w/\rho}$ (ρ is the fluid density and τ_w is the time-averaged streamwise wall shear stress; the spanwise component is zero) and the kinematic viscosity ν.

The interaction between the coherent Stokes layer and the stochastic near-wall turbulence influences the main structures of the near-wall cycle, i.e. the low-speed streaks and the quasi-streamwise vortices, eventually yielding a reduction of turbulent friction. When the Reynolds number based on the friction velocity is $Re_\tau = 200$, the largest drag reduction rate for a given oscillation amplitude $A^+ = 12$ is approximately 45 %, obtained for the optimal actuation period $T^+ \approx 100$ (Quadrio & Ricco 2004). Larger or smaller periods result in smaller drag reduction. Several authors, for example Yakeno, Hasegawa & Kasagi (2014), observed that the orientation of near-wall structures in wall-parallel planes is cyclically altered by the coherent spanwise shear. Touber & Leschziner (2012) have shown that, provided the time scale of the spanwise shear oscillation is short enough, the low-speed streaks do not have the time to fully reorient during the oscillation, and are thus weakened. Hence, at the root of drag reduction lies the interaction between the oscillating shear (a coherent component) and the natural streak regeneration mechanism (seen in the stochastic component).

Touber & Leschziner (2012) and later Agostini *et al.* (2014) applied a triple decomposition of the velocity field to the budgets of the single-point Reynolds stresses; the turbulent (stochastic) fluctuations were isolated and their interaction with the (coherent) Stokes layer was studied. It was found that the interaction between coherent and stochastic fields is mediated by the interplay between the coherent spanwise shear $\partial\tilde{w}/\partial y$ and the

$\overline{v''w''}$ component of the Reynolds stress tensor, induced by the rotation of the vortical structures. For nearly optimal periods, the interaction between the coherent and stochastic fields is a one-way interaction, with the former altering the latter. This weakens the wall-normal velocity fluctuations and reduces the turbulent shear, reducing eventually the friction drag. For larger periods, instead, the interaction becomes a two-way interaction, with coherent and stochastic fields mutually exchanging energy. In this case, however, the drag reduction effect is less important. By looking at different phases along the period, they found that, when large, the Stokes shear $\partial\tilde{w}/\partial y$ changes relatively slowly in time and allows the structures to become more vigorous and well-established (a process they referred to as lingering). Conversely, when $\partial\tilde{w}/\partial y$ is small, the structures appear weak and less tilted.

In this example, we intend to add scale information to the picture. We thus apply the φAGKE: (i) to describe the influence of the coherent motion on the spatial arrangement of the near-wall structures during the control period, (ii) to inspect the mean–coherent–stochastic interaction in the scale space and in physical space and (iii) to characterise the phase dependence of the interaction between the coherent and stochastic fields.

3.1. *Database and computational details*

The φAGKE terms are computed from two datasets obtained by direct numerical simulations. They are described by Gallorini, Quadrio & Gatti (2022), where the interested reader can find full details.

The simulations are run under a constant pressure gradient (Quadrio, Frohnapfel & Hasegawa 2016), with a friction Reynolds number of $Re_\tau = u_\tau h/\nu = 200$, where h is the channel half-height. A constant pressure gradient provides a unique value of u_τ with/without drag reduction, thus avoiding ambiguities in viscous scaling. The size of the computational domain is $(L_x, L_y, L_z) = (4\pi h, 2h, 2\pi h)$ in the streamwise, wall-normal and spanwise directions. The number of Fourier modes is $N_x = N_z = 256$ in the two homogeneous (streamwise and spanwise) directions, further increased by a factor of 3/2 to remove aliasing error. In the wall-normal direction, a hyperbolic tangent distribution of $N_y = 192$ points provides a finer grid near the wall. The spatial resolution is $\Delta x^+ = 6.6$ and $\Delta z^+ = 3.3$ by considering the extra modes, while Δy^+ varies from $\Delta y^+ \approx 0.5$ close to the wall to $\Delta y^+ \approx 3.7$ at the centreline.

A first simulation of a plane channel with fixed walls is run as a reference, followed by two others in which wall oscillation according to (3.1) is enforced. The oscillation amplitude is fixed at $A^+ = 7$: a rather small value, which keeps the energy cost of the actuation limited, and might even provide a small net energy saving at optimal periods. As in Agostini & Leschziner (2014), we consider two control periods, namely $T^+ = 75$ and $T^+ = 250$. The value $T^+ = 75$ is nearly optimal, and yields drag reduction (defined here as a percentage decrease of the friction coefficient, determined by the increase in bulk velocity) of 25.2 %. The value $T^+ = 250$ is suboptimal, and yields only 13.2 % drag reduction. These figures are in agreement with existing information (see e.g. Gatti & Quadrio 2016).

Simulations are started from an uncontrolled turbulent flow field. During the initial, transient phase, the solution is advanced by setting the Courant–Friedrichs–Lewy number at 1. After the transient, however, the time step is set to a fixed value, in order to synchronise data saving with predetermined control phases. The value of the time step is thus chosen as an integer submultiple of the forcing period that keeps the maximum Courant–Friedrichs–Lewy number below unity: it is $\Delta t^+ = 0.0938$ for the smaller period

and $\Delta t^+ = 0.0781$ for the longer period. After the transient, 376 complete velocity fields are saved, so that 47 control periods are stored for later analysis, each of them divided in 8 equally spaced phases.

The φAGKE terms are computed from the database with a post-processing code derived with modifications from that described by Gatti *et al.* (2020). It employs the same important numerical optimisations described in Gatti *et al.* (2019), which include the computation of correlations pseudo-spectrally whenever possible. The code, written in the CPL computer programming language (Luchini 2020, 2021), has been validated by checking that the sum of each term of the budget of coherent and stochastic fields equals the corresponding term of $\langle \delta u_i' \delta u_j' \rangle$ within round-off. Statistical convergence of the results is verified by ensuring that the residuals of the budgets are negligible compared with the values of the production, pressure–strain and dissipation.

3.2. *The φAGKE tailored to channel flow with oscillating walls*

The general form (2.17) and (2.18) of the φAGKE can be simplified for the problem at hand. Since x and z are homogeneous, in an indefinite plane channel the φAGKE depend on five independent variables: the three components of the separation vector (r_x, r_y, r_z), the wall-normal component of the midpoint Y and the phase φ. Note that the finite distance between the two walls implies the constraint $r_y < 2Y$.

In an indefinite channel flow, the x direction aligns with the mean flow, hence $\boldsymbol{U}(y) = (U(y), 0, 0)$, and the wall-parallel derivatives of the mean velocity are zero. Moreover, in the specific case of the oscillating wall, the coherent velocity field is independent on x and z, as the wall control law (3.1) is a function of time only, so that $\partial \tilde{u}_i/\partial x = \partial \tilde{u}_i/\partial z = 0$. Therefore, incompressibility and no penetration at the wall dictate that the wall-normal component of the coherent field is null everywhere, i.e. $\tilde{v}(y, t) = 0$. The streamwise coherent velocity $\tilde{u}$, instead, does not vanish, albeit it is known to be extremely small: (Yakeno *et al.* 2014) report it to be two orders of magnitude smaller than the spanwise coherent velocity $\tilde{w}$. The non-zero components of the $\delta\tilde{u}_i\delta\tilde{u}_j$ tensor are $\delta\tilde{u}\delta\tilde{u}$, $\delta\tilde{w}\delta\tilde{w}$ and $\delta\tilde{u}\delta\tilde{w}$.

The specialised form of the φAGKE for the channel flow with oscillating walls is reported in Appendix B. It can be observed that the mean–coherent production p_{ij}^{mc} is zero: in this particular case, there is no exchange of stresses between the mean and coherent fields, as the coherent field interacts directly with the external forcing and with the stochastic field only. However, this term does appear in other flows, and for example is important for the flow past a bluff body (Alves Portela *et al.* 2020), where the mean flow supports the coherent vortex shedding, which in turn supports the stochastic fluctuations. In the budget for the stochastic part, the productions p_{ij}^{ms} and p_{ij}^{cs} represent the two avenues for the stochastic field to interact with the mean and coherent fields, involving distinct components of $\overline{\delta u_i'' \delta u_j''}$. The mean–stochastic production p_{ij}^{ms} is non-zero only for $\overline{\delta u'' \delta u''}$ and for the off-diagonal components $\overline{\delta u'' \delta v''}$ and $\overline{\delta u'' \delta w''}$. In contrast, the coherent–stochastic production contributes to all the elements of $\overline{\delta u_i'' \delta u_j''}$ except for $\overline{\delta v'' \delta v''}$, being $p_{22}^{cs} = 0$.

The flow symmetries and the type of forcing make only certain paths available for energy exchanges. This is represented graphically in figure 3, which shows an 'energy circle' (Quadrio 2011) to describe energy exchanges among the mean, coherent and stochastic fields after spatial and temporal integration. In the following, thanks to the φAGKE, these

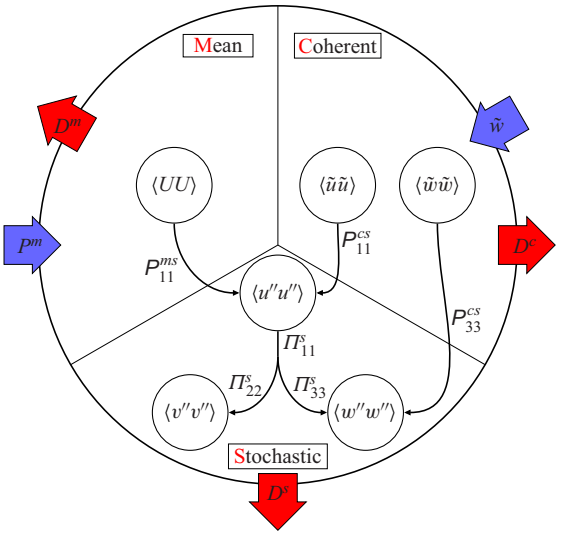

Figure 3. Sketch of the energy exchanges between mean, coherent and stochastic fields for the turbulent channel flow modified by spanwise-oscillating walls. Blue (red) arrows indicate energy entering (leaving) the system. The blue arrows P_m and $\tilde{w}$ represent the pumping energy required to move the flow, and the energy introduced by the moving walls.

global energy exchanges and redistributions are expanded and described in space and among scales, with a phase-by-phase analysis.

4. Effect of the spanwise forcing on the near-wall cycle

The influence of the oscillating wall on the structural organisation of the stochastic part of the velocity fluctuations in the near-wall region is considered first, at a single phase and then in terms of its phase evolution. The energy exchanges among mean, coherent and stochastic fields are then addressed, followed by the analysis of the pressure–strain redistribution. Eventually, the influence of the Stokes layer and the stochastic pressure–strain term π^s_{33} on the transfer of the spanwise stochastic stresses is described.

4.1. *Near-wall structures*

4.1.1. *Description at a fixed phase*

Figure 4 shows the diagonal components of $\overline{\delta u_i'' \delta u_j''}$ in the $r_y = r_x = 0$ plane for the uncontrolled channel (figure 4*a–c*), $T^+ = 75$ (figure 4*d–f*) and $T^+ = 250$ (figure 4*g–i*). For the two controlled cases, only phase φ_4 is shown, but the discussion that follows is qualitatively valid for all phases.

The local maxima of $\overline{\delta u'' \delta u''}$ and $\overline{\delta v'' \delta v''}$, hereafter denoted with subscript m, are the statistical trace of the structures of the near-wall cycle. In the $r_x = r_y = 0$ space, indeed, they indicate a negative peak of the streamwise and vertical stochastic correlation functions R_{11} and R_{22}; see (2.7). The coordinates $Y^+ \approx 14$–18 and $r_z^+ \approx 55$–65 of $\overline{\delta u'' \delta u''}_m$ in the (r_z^+, Y^+) plane indicate the characteristic wall distance and spanwise spacing of low- and high-speed streaks. The coordinates $Y^+ \approx 43$–55 and $r_z^+ \approx 49$–59 of $\overline{\delta v'' \delta v''}_m$ indicate

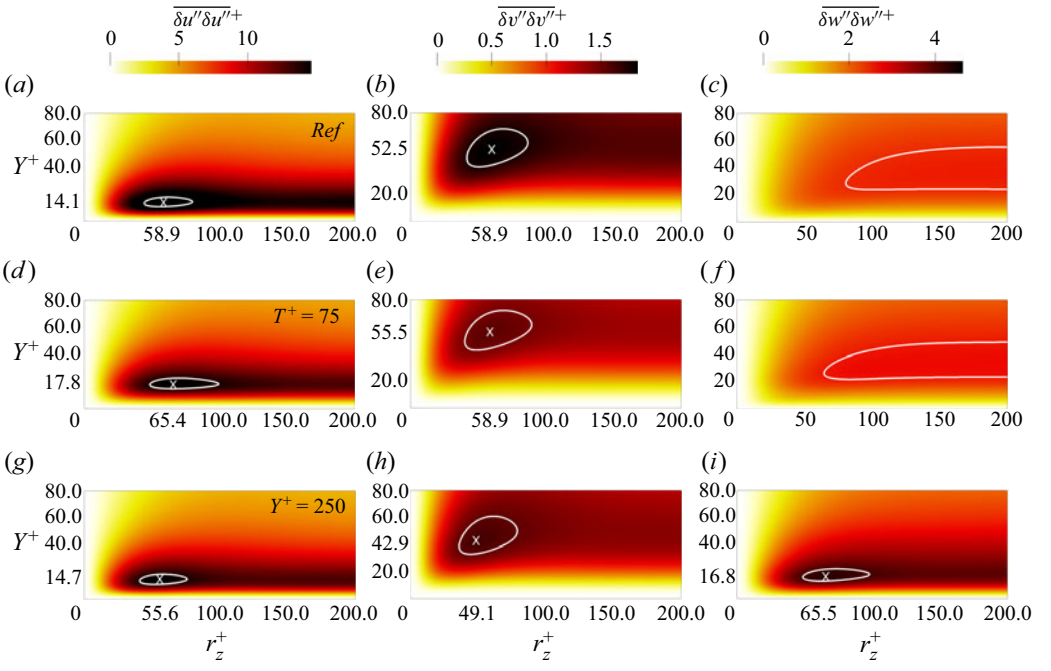

Figure 4. Diagonal components of the stochastic tensor $\overline{\delta u_i'' \delta u_j''}^+$ at φ_4 in the (r_z^+, Y^+) plane. (*a–c*) Uncontrolled case with $A = 0$, (*d–f*) $T^+ = 75$ and (*g–i*) $T^+ = 250$. The contour is set at 95 % of each maximum. The coordinates of the maximum, marked with a cross, can be read on the axes.

the characteristic wall distance and spanwise size of the quasi-streamwise vortices, which induce at their spanwise sides regions of vertical velocity with negative correlation.

Figure 4 shows that the oscillating wall leaves $\overline{\delta u''\delta u''}$ and $\overline{\delta v''\delta v''}$ almost unchanged, indicating that the size and strength of the near-wall structures only marginally depend on the amount of drag reduction.

This is consistent with the constant pressure gradient driving strategy, which forces the same level of wall friction; the large changes observed by various authors under different driving strategies simply derive trivially from the different friction, as discussed by Frohnapfel, Hasegawa & Quadrio (2012). However, the velocity streaks are slightly moved away from the wall: an upward shift of $\overline{\delta u''\delta u''}_m$ can be seen in figure 4. The previous observation is confirmed by numerical data: the maximum moves from $Y^+ = 14.1$ in the reference case to $Y^+ = 17.8$ for $T^+ = 75$ and to $Y^+ = 14.7$ for $T^+ = 250$ (at phase φ_4). Both shifts are upwards, and the $T^+ = 75$ case with larger drag reduction has a larger shift. The quasi-streamwise vortices react differently from control: $\overline{\delta v''\delta v''}_m$ moves from $Y^+ = 53$ in the reference case to $Y^+ = 55$ for $T^+ = 75$ and to $Y^+ = 43$ for $T^+ = 250$. These contrasting trends are consistent with the wall-normal displacement found by Gallorini *et al.* (2022) for conditionally averaged quasi-streamwise vortices, but are extracted from the present analysis without the need for an (inevitably subjective) procedure for conditional structure extraction.

In the canonical channel flow, the map of $\overline{\delta w''\delta w''}$ embeds information of the quasi-streamwise vortices only when the $r_y \neq 0$ space is considered, which contains the peak $\langle \delta w' \delta w' \rangle_m$ (Gatti *et al.* 2020). Indeed, the quasi-streamwise vortices induce negatively correlated regions of w'' fluctuations at their vertical sides only, and the r_y coordinate of the

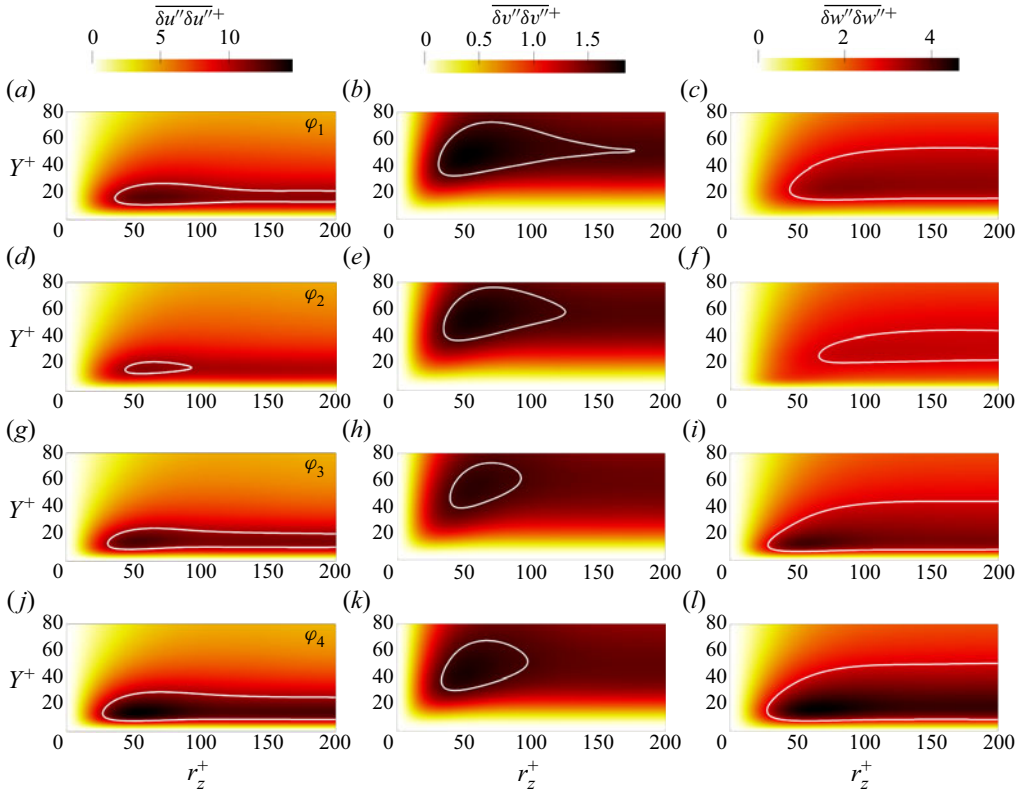

Figure 5. Diagonal components of the stochastic tensor $\overline{\delta u_i'' \delta u_j''}^+$ in the (r_z^+, Y^+) plane, at phases (*a–c*) φ_1, (*d–f*) φ_2, (*g–i*) φ_3 and (*j–l*) φ_4, for the period $T^+ = 250$. For each component, the white contour is set at the 95 % of the smallest peak over the phases (i.e. at φ_2 for $\overline{\delta u''\delta u''}$ and $\overline{\delta w''\delta w''}$, and at φ_3 for $\overline{\delta v''\delta v''}$).

maximum indicates their characteristic wall-normal size. In the controlled cases, however, a local peak of $\overline{\delta w''\delta w''}$ appears in the $r_x = r_y = 0$ (figure 4) and $r_z = r_y = 0$ (not shown) planes. Interestingly, the local peak is particularly evident for $T^+ = 250$, extending for $r_z^+ \approx 50$–100, $r_x^+ \approx 85$–270 and $Y^+ \approx 13$–25, but it is hardly visible for $T^+ = 75$, where the w'' fluctuations are weaker. The next subsection, which examines how these quantities vary with φ, shows that this derives from a combination of the streaks tilting in the x–z plane and from the interaction of the quasi-streamwise vortices with the coherent spanwise shear.

4.1.2. *Evolution during the cycle*

Figure 5 shows the phase evolution of $\overline{\delta u''\delta u''}$, $\overline{\delta v''\delta v''}$ and $\overline{\delta w''\delta w''}$ in the $r_x = r_y = 0$ plane, to describe how the organisation of the near-wall stochastic fluctuations changes during the oscillation cycle, i.e. the very type of information that the φAGKE are designed to provide. Only the suboptimal $T^+ = 250$ is considered, as the large period emphasises the phase dependence; moreover, only one half of the forcing period is shown (from φ_1 to φ_4), because of temporal symmetry. Extra quantitative information is provided by figure 6, which plots the phase evolution of the maxima $\overline{\delta u''\delta u''}_m$, $\overline{\delta v''\delta v''}_m$ and $\overline{\delta w''\delta w''}_m$.

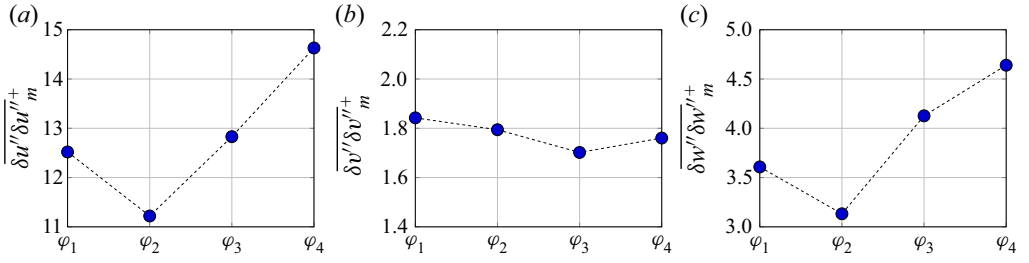

Figure 6. (*a–c*) Phase variation of the maxima $\overline{\delta u_i''\delta u_i''}^+_m$ in the (r_z^+, Y^+) plane.

The streamwise velocity streaks cyclically strengthen and weaken under the action of the alternating Stokes layer. The maximum $\overline{\delta u''\delta u''}_m$ assumes its lowest value at φ_2, and then grows to reach the highest value at φ_4, with an intra-cycle variation of 27 %. The quasi-streamwise vortices, instead, show a much smaller phase dependence: the intra-cycle variation of $\overline{\delta v''\delta v''}$ is 8 % only. This is not surprising, since the quasi-streamwise vortices reside at larger wall distances, where the intensity of the Stokes layer is lower; at $y^+ = 14$, the average position of the streaks, the maximum $\tilde{w}^+$ is 1.15, while at $y^+ = 50$, representative wall-normal distance of the vortices, it is only 0.2. A different wall distance for streaks and vortices also implies a phase shift; in fact the intensity of $\overline{\delta v''\delta v''}$ is minimum at φ_3 and maximum at φ_1, whereas $\overline{\delta u''\delta u''}$ and $\overline{\delta w''\delta w''}$ are minimum at φ_2 and maximum at φ_4. This is consistent with the early observation (Baron & Quadrio 1996) that streaks and quasi-streamwise vortices are displaced by the spanwise Stokes layer differently.

From figure 6, one notices that the phase evolution of $\overline{\delta w''\delta w''}_m$ resembles that of $\overline{\delta u''\delta u''}_m$, thus suggesting that part of the stochastic w'' fluctuations derives from a redistribution of the streamwise fluctuations. The near-wall structures are tilted in the x–z plane and follow the shear vector $(\mathrm{d}U/\mathrm{d}y, 0, \partial\tilde{w}/\partial y)$ (Yakeno *et al.* 2014). The tilting causes the streamwise high- and low-speed streaks to reorient, thus contributing via pressure–strain redistribution (see below § 4.3) to the spanwise stochastic fluctuations. When the tilting angle is positive (negative), the low- and high-speed streaks contribute to respectively positive (negative) and negative (positive) w''. This produces regions of w'' fluctuations that correlate negatively for scales r_x and r_z and position Y compatible with the position of $\overline{\delta w''\delta w''}_m$ observed in figure 5. This is shown with a sketch in figure 7, and confirmed with a phase-by-phase conditional average of events extracted from the present database in Appendix C. The picture is also consistent with the lower $\overline{\delta w''\delta w''}_m$ observed in figure 4 for $T^+ = 75$: for periods close to the optimum, the oscillation is too fast for the streaks to align with the shear vector (Touber & Leschziner 2012), and this redistribution mechanism becomes weaker.

Similar information is usually extracted (Yakeno *et al.* 2014) from phase-locked conditional averages. However, such statistics are unavoidably arbitrary to some degree; e.g. 'short' structures have to be excluded from averaging, and one needs to predetermine a specific wall distance for the eduction procedure. Here we obtain information that is equivalent to conditional averaging, but via a statistical analysis that is free from assumptions and hypotheses.

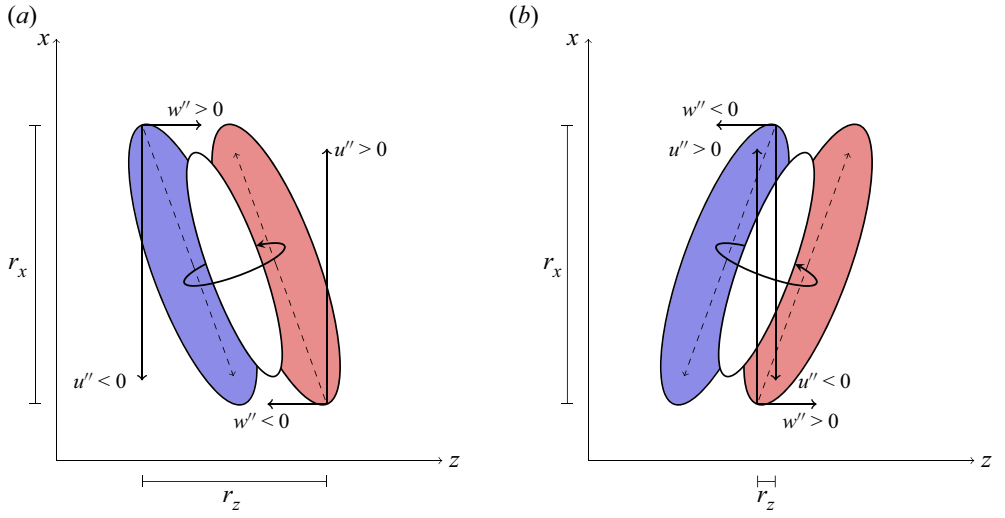

Figure 7. Sketch of the contribution of u'' and w'' for positively (*a*) and negatively (*b*) tilted low-speed (blue) and high-speed (red) streaks induced by a positively rotating quasi-streamwise vortex (white).

For example, the scales $r_{z,m}$ and $r_{x,m}$ identified by $\overline{\delta w''\delta w''}_m$ can be used to track the phase evolution of the tilting angle θ of the flow structures during the cycle:

$$|\theta(\varphi)| = \tan^{-1}\left(\frac{r_{z,m}(\varphi)}{r_{x,m}(\varphi)}\right). \tag{4.1}$$

Similarly, the evolution of the wall-normal position Y_m of $\overline{\delta w''\delta w''}_m$ (or, equivalently, of $\overline{\delta u''\delta u''}_m$) quantifies the vertical displacement of the streaks during the cycle.

Figure 8 compares $|\theta|$ with the shear angle θ_s evaluated at Y_m, i.e.

$$\theta_s = \tan^{-1}\left(\frac{\partial\tilde{w}/\partial y}{\mathrm{d}U/\mathrm{d}y}\right), \tag{4.2}$$

that is conventionally used to describe the tilting angle of the near-wall structures (Yakeno *et al.* 2014; Gallorini *et al.* 2022). The two quantities θ and θ_s are quantitatively similar and present the same phase dependence, with a nearly constant difference of approximately 8°. Figure 8(*b*) also shows that when the tilting angle of the streaks is maximum, their distance from the wall is minimum (and vice versa). This implies that a higher coherent spanwise velocity yields a larger tilting.

Part of the wall-parallel modulation of $\overline{\delta w''\delta w''}$ induced by the wall oscillation derives from the interaction of the quasi-streamwise vortices with the coherent spanwise shear. When the coherent shear $\partial\tilde{w}/\partial y$ is positive, the quasi-streamwise vortices move low-spanwise-velocity fluid upwards, and high-spanwise-velocity fluid downwards. The opposite happens when $\partial\tilde{w}/\partial y < 0$. This creates two regions with spanwise velocity of opposite sign at the vortex sides, resulting in negative R_{33} correlation and a positive peak of $\overline{\delta w''\delta w''}$ at their characteristic spanwise separation. This process, quantified by the coherent–stochastic production p_{33}^{cs} (see § 4.2), resembles the ejections and sweeps typical of the near-wall cycle, where the mean streamwise shear is involved; its description is similar to the explanation provided by Agostini *et al.* (2014) for the non-zero $\langle v''w''\rangle$. Once again, our interpretation is supported by the velocity field induced by the

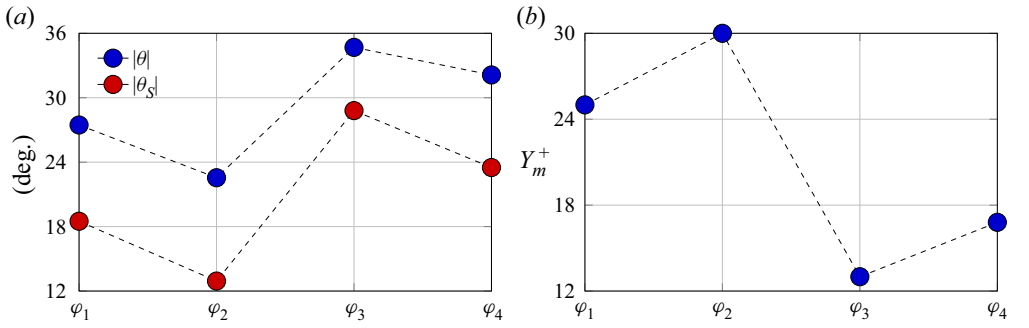

Figure 8. (*a*) Evolution of the tilt angle of the wall streaks during the cycle. Comparison between present results (blue symbols) and the shear angle introduced by Yakeno *et al.* (2014) (red symbols). (*b*) Wall-normal position of the structures, educed from the wall-normal position Y_m^+ of $\overline{\delta w'' \delta w''}_m$.

ensemble-averaged quasi-streamwise vortex, computed at various phases and shown in Appendix C.

4.2. *Interaction of the mean, coherent and fluctuating fields*

The energy exchanges of the mean field with the stochastic and coherent fields are described by the two mean production terms p_{ij}^{mc} and p_{ij}^{ms}. However, as shown in figure 3, for the present problem $p_{ij}^{mc} = 0$, and the mean field interacts directly with the stochastic field only, by feeding (or draining from) streamwise fluctuations. Moreover, energy is exchanged between the coherent and stochastic fields via the coherent–stochastic production p_{ij}^{cs}, which involves only $\overline{\delta u'' \delta u''}$ and $\overline{\delta w'' \delta w''}$ among the diagonal components of the $\overline{\delta u_i'' \delta u_j''}$ tensor.

Figure 9 shows how the mean–stochastic production p_{11}^{ms} varies with φ for $T^+ = 75$ (figure 9*a*,*c*,*e*,*g*) and $T^+ = 250$ (figure 9*b*,*d*,*f*,*h*) in the $r_x = r_y = 0$ plane, where the production terms are maxima. Here, p_{11}^{ms} reduces to

$$p_{11}^{ms} = -2\overline{\delta u'' \delta v''} \left(\frac{\mathrm{d}U}{\mathrm{d}y} \right). \tag{4.3}$$

The mean–stochastic production is positive everywhere, with a peak in the range $r_{z,m}^+ = 36$–42 and $Y_m^+ = 13$–17 for $T^+ = 75$ and $r_{z,m}^+ = 36$–39 and $Y_m^+ = 12$–14 for $T^+ = 250$. Hence, the interaction of the near-wall cycle ($\overline{\delta u'' \delta v''}$) with the mean shear ($\mathrm{d}U/\mathrm{d}y$) invariably moves energy from the mean field towards the stochastic streamwise fluctuations. Note that the smaller Y^+ for $T^+ = 250$ is consistent with the reduced thickening of the viscous sublayer for suboptimal periods. The production intensity is largest at φ_1 and lowest at φ_3 for $T^+ = 75$, whereas it is largest at φ_3 and lowest at φ_1 for $T^+ = 250$. Since $\mathrm{d}U/\mathrm{d}y$ is phase-independent, this can only descend from $\overline{\delta u'' \delta v''}$, which includes the phase evolution of the streaks and of the quasi-streamwise vortices (see § 4.1.2).

Figures 10 for $T^+ = 75$ and 11 for $T^+ = 250$ show how p_{11}^{cs} and p_{33}^{cs} change with φ. Like for p_{11}^{ms}, the expressions for p_{11}^{cs} and p_{33}^{cs} simplify in the $r_x = r_y = 0$ plane where their maxima occur, i.e.

$$p_{11}^{cs} = -2\overline{\delta u'' \delta v''} \left(\frac{\partial \tilde{u}}{\partial y} \right) \quad \text{and} \quad p_{33}^{cs} = -2\overline{\delta v'' \delta w''} \left(\frac{\partial \tilde{w}}{\partial y} \right). \tag{4.4a,b}$$

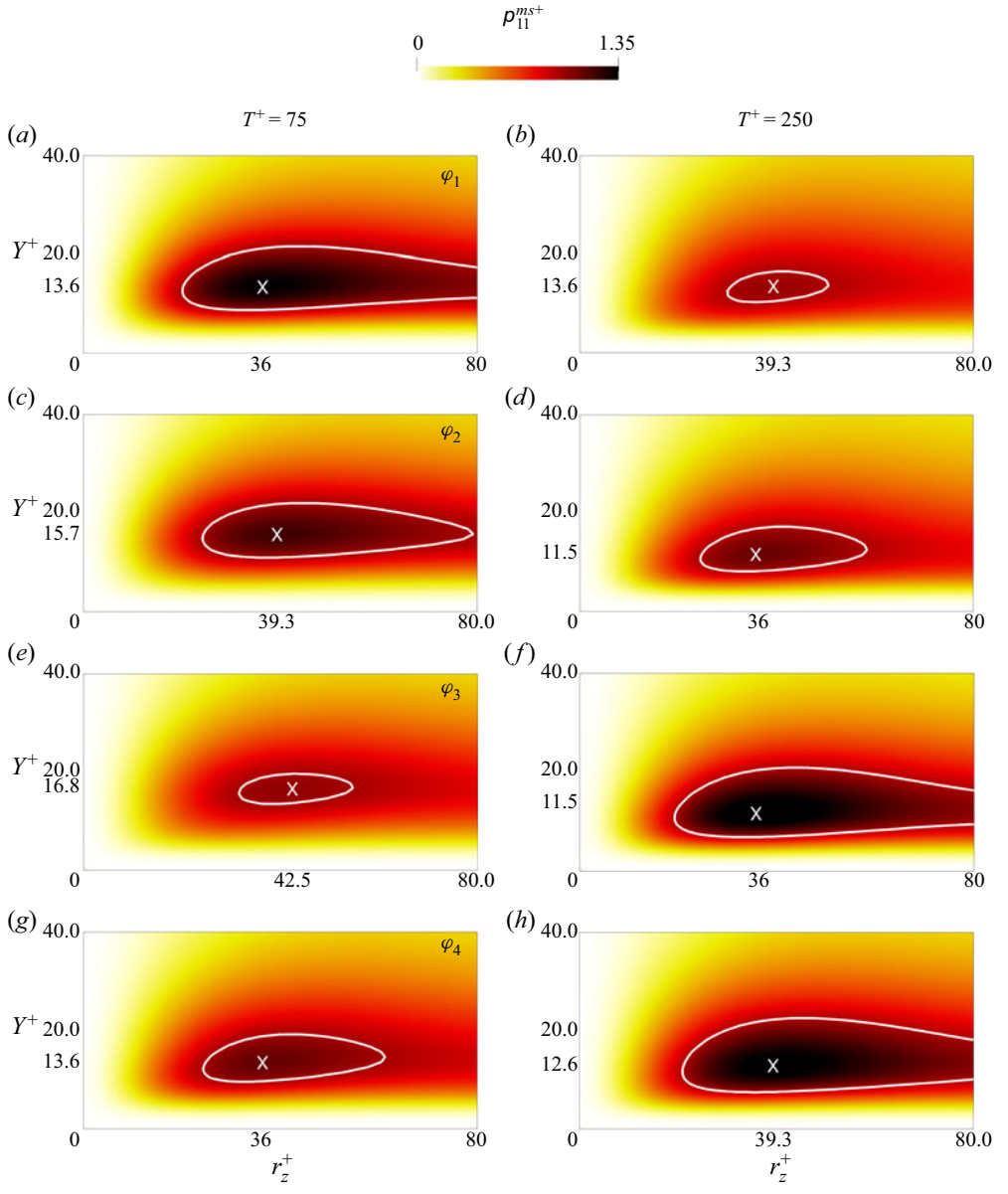

Figure 9. Mean–stochastic production p_{11}^{ms+} in the (r_z^+, Y^+) plane for $T^+ = 75$ (*a*,*c*,*e*,*g*) and $T^+ = 250$ (*b*,*d*,*f*,*h*), at phases (*a*,*b*) φ_1, (*c*,*d*) φ_2, (*e*,*f*) φ_3 and (*g*,*h*) φ_4. The contour line is set at 95 % of the smallest maximum over the phases. The coordinates of the maximum, marked with a cross, can be read on the axes.

Unlike p_{11}^{ms}, however, these productions can take either sign. Their maps show evident horizontal stripes of alternating sign, from the wall up to $Y^+ \approx 40$: hence, at a given phase the coherent field feeds the stochastic field at certain wall distances, but extracts energy from it at others. It is worth noting that, although p_{11}^{cs} and p_{33}^{cs} at a given phase are both positive and negative, after averaging over the phases $\langle p_{11}^{cs} \rangle$ almost vanishes and $\langle p_{33}^{cs} \rangle$ is positive everywhere. This is not entirely new, and confirms the single-point analysis by Agostini *et al.* (2014) (see their figure 14); however, scale information is added here

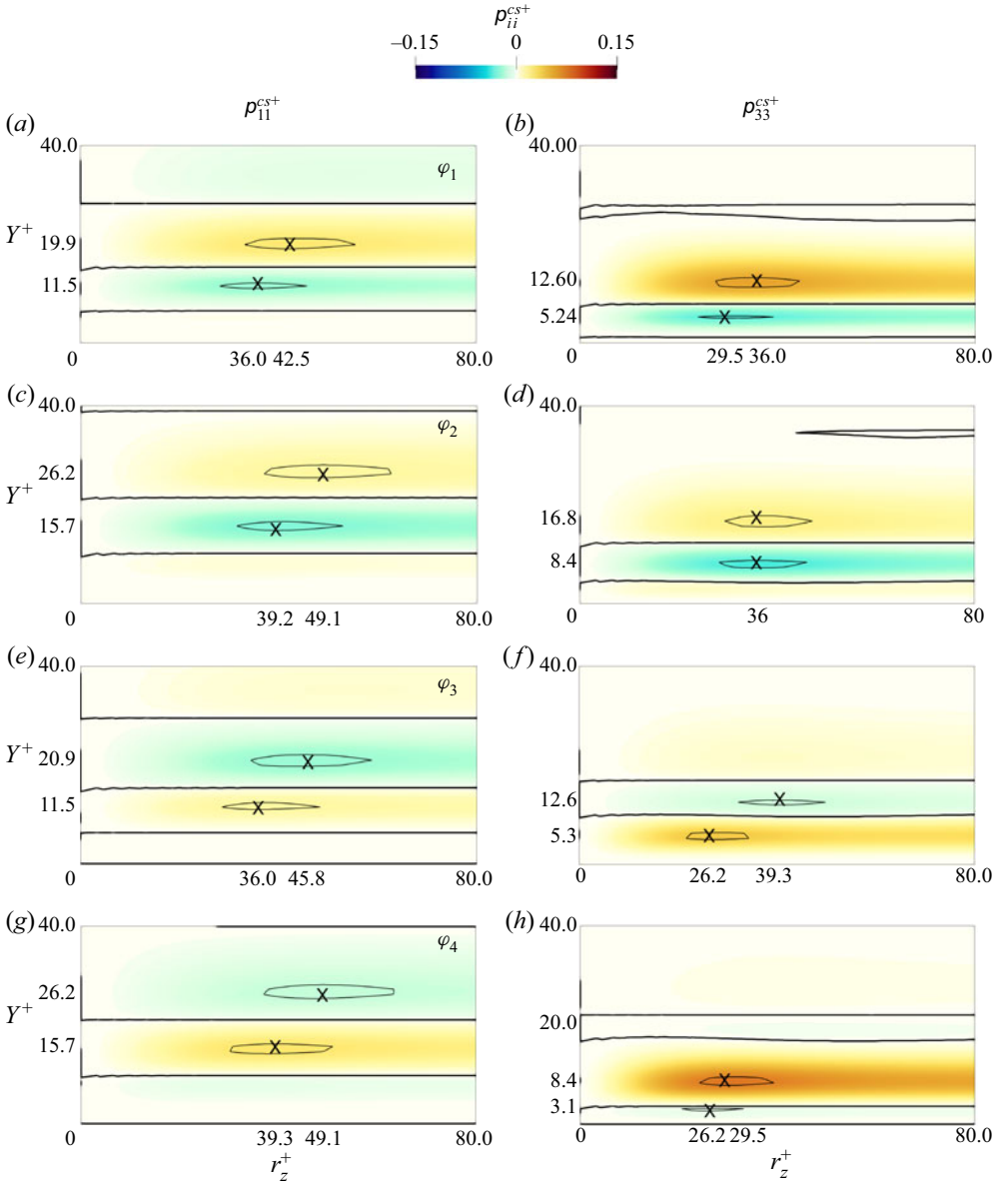

Figure 10. Coherent–stochastic production p_{11}^{cs+} (*a*,*c*,*e*,*g*) and p_{33}^{cs+} (*b*,*d*,*f*,*h*) in the (r_z^+, Y^+) plane for $T^+ = 75$, at phases (*a*,*b*) φ_1, (*c*,*d*) φ_2, (*e*,*f*) φ_3 and (*g*,*h*) φ_4. The thin contour line is set at 95 % of the smallest (positive and negative) maximum over the phases; the thick black contour line is $p_{ii}^{cs} = 0$. The coordinates of the maximum, marked with a cross, can be read on the axes.

so that this mechanism can be related to the structures of the flow. At every phase, the positive/negative peaks of p_{11}^{cs} and p_{33}^{cs} occur at $r_z^+ \approx 25$–50, a spanwise separation which points to the structures of the near-wall cycle.

The intensity of p_{11}^{cs} and p_{33}^{cs} at the two periods is comparable, at all scales and positions. However, for p_{11}^{cs} the contribution of the shear stresses is dominant, whereas the opposite occurs for p_{33}^{cs}, where the coherent spanwise shear dominates. Indeed, $\partial\tilde{w}/\partial y$ is two

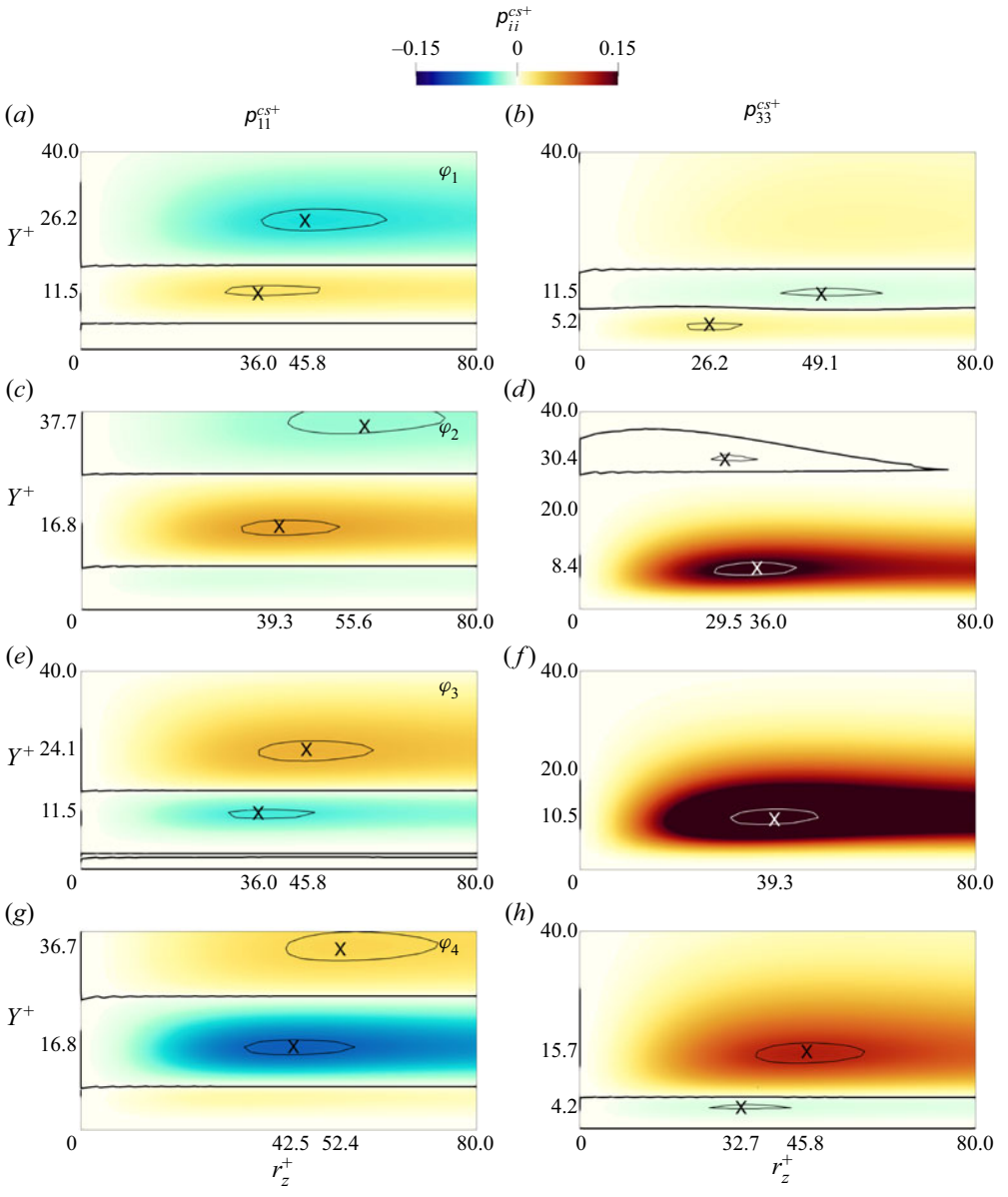

Figure 11. As in figure 10, but for $T^+ = 250$.

orders of magnitude larger than $\partial\tilde{u}/\partial y$, and $\overline{\delta v''\delta w''}$ is two orders of magnitude smaller than $\overline{\delta u''\delta v''}$. Note, moreover, that for both control periods $p_{11}^{ms} \gg p_{11}^{cs}$, meaning that the streamwise stochastic fluctuations are predominantly fed by the mean field.

The alternating positive/negative stripes for p_{11}^{cs} and p_{33}^{cs} are due to the change of sign of $\partial\tilde{u}/\partial y$ and $\partial\tilde{w}/\partial y$ with y. For p_{33}^{cs}, the changing sign of the shear is also indirectly responsible for the alternating positive/negative $\overline{\delta v''\delta w''}$, due to the quasi-streamwise vortex–shear interaction described in § 4.1.2. In contrast, for p_{11}^{cs}, $\overline{\delta u''\delta v''}$ is entirely due to

the interaction of the near-wall structures with the mean shear $\mathrm{d}U/\mathrm{d}y$, which overwhelms $\partial\tilde{u}/\partial y$ everywhere.

Comparing figures 10 and 11 highlights that the slower oscillation introduces substantial differences in the coherent–stochastic energy exchange. The positive/negative maxima of p_{11}^{cs} increase, and their positions move towards larger r_z and larger Y, but the effect of T^+ on p_{33}^{cs} is even more evident. At $T^+ = 250$, the stripes of negative p_{33}^{cs} weaken, while those with $p_{33}^{cs} > 0$ strengthen; overall, the spanwise contribution to the energy flowing from the coherent to the stochastic field becomes larger. A larger oscillating period implies a larger thickness of the Stokes layer, proportional to $\sqrt{\nu T}$, thus stretching outwards the coherent spanwise shear and, as a consequence, the scale-space map of $\overline{\delta v'' \delta w''}$, yielding an overall increase of the positive p_{33}^{cs}. At φ_2 and φ_3, for example, $\partial\tilde{w}/\partial y$ is negative close to the wall and changes sign only at $y^+ \approx 30$–50 for $T^+ = 250$ (see figure 2), while it changes sign already at $y^+ \approx 13$–18 for $T^+ = 75$ (not shown). For $T^+ = 250$ this results in a large increase of the near-wall positive p_{33}^{cs}, as highlighted by the dark red colour in figure 11. Due to the negative $\partial\tilde{w}/\partial y$, indeed, the quasi-streamwise vortices induce on their sides positive/negative v'' and convect upwards/downwards high/low spanwise velocity w'', thus yielding positive $\overline{\delta v'' \delta w''}$ and an intense energy exchange from the coherent to the stochastic field. The scale-space information of this exchange mechanism is highlighted by the positive peak of p_{33}^{cs} placed at $(r_z^+, Y^+) \approx (38, 9)$ for the considered φ_2 and φ_3 phases.

4.3. *Pressure–strain redistribution*

As seen schematically in figure 3, the pressure–strain action partially redistributes the streamwise energy $\overline{\delta u'' \delta u''}$ drained from the mean flow towards the cross-stream fluctuations $\overline{\delta v'' \delta v''}$ and $\overline{\delta w'' \delta w''}$. Figure 12(*a*,*c*,*e*) shows that $\pi_{11}^s < 0$, $\pi_{22}^s > 0$ and $\pi_{33}^s > 0$ at almost all scales and positions: only in a very thin region close to the wall are $\pi_{11}^s > 0$, $\pi_{22}^s < 0$ and $\pi_{33}^s > 0$, according to the reorientation of vertical fluctuations into wall-parallel ones because of the impermeable wall (Mansour, Kim & Moin 1988). The peaks of π_{11}^s, π_{22}^s and π_{33}^s in the (r_z, Y) plane have $Y_m^+ \approx 11$–27 and $r_{z,m}^+ \approx 30$–52, indicating that the energy redistribution is dominated by the near-wall cycle.

It is known (Touber & Leschziner 2012; Yakeno *et al.* 2014) that the spanwise oscillation of the wall enhances the energy redistribution, mainly towards spanwise fluctuations. Compared with the uncontrolled case, the negative peak of π_{11}^s increases by 23 %–67 % for $T^+ = 75$ and by 36 %–77 % for $T^+ = 250$, while the positive peak of π_{22}^s decreases by 2 %–11 % for $T^+ = 75$ and increases by 4 %–29 % for $T^+ = 250$. The positive peak of π_{33}^s, instead, has the largest variation, with an increase of 30 %–53 % for $T^+ = 75$ and 40 %–87 % for $T^+ = 250$.

The phase evolution of the pressure-mediated energy redistribution is described in figure 12(*b*,*d*,*f*) for the $T^+ = 250$ case, by considering the maxima of the diagonal components of π_{ij}^s. Only their values are plotted, since their position remains nearly constant at $(Y^+, r_z^+) \approx (20, 52)$ for $\pi_{11,m}^s$, $\approx (27, 30)$ for $\pi_{22,m}^s$ and $\approx (12, 46)$ for $\pi_{33,m}^s$. Like $\overline{\delta v'' \delta v''}_m$, $\pi_{22,m}^s$ is the component with the smallest intra-cycle variation, with a 21 % excursion during the cycle compared with 30 % and 35 % for $\pi_{11,m}^s$ and $\pi_{33,m}^s$. In fact, the largest energy redistribution towards $\overline{\delta v'' \delta v''}$ occurs quite far from the wall, where the influence of the Stokes layer is weak. The phase dependence of $\pi_{11,m}^s$ is qualitatively different from that of the others. The redistribution of $\overline{\delta u'' \delta u''}$ towards the cross-stream components is maximum at φ_3 and minimum at φ_1, following the absolute value of $\pi_{11,m}^s$.

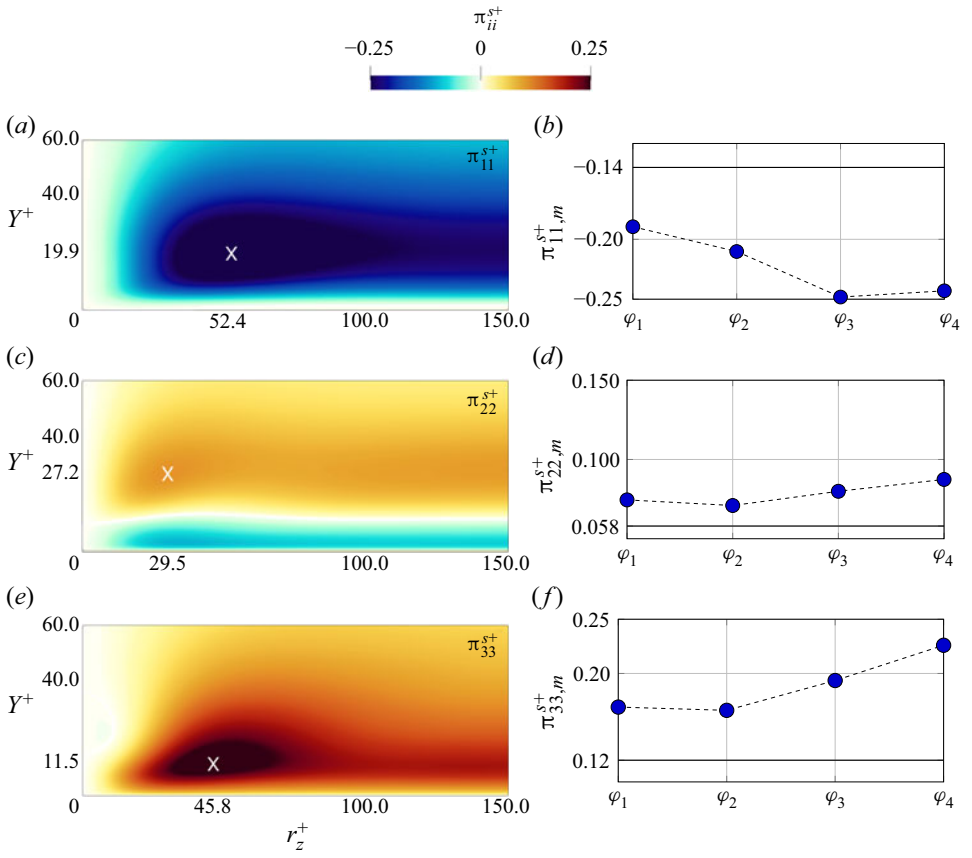

Figure 12. (*a*,*c*,*e*) Pressure–strain redistribution π_{ii}^{s+} from $\overline{\delta u''\delta u''}$ towards $\overline{\delta v''\delta v''}$ and $\overline{\delta w''\delta w''}$ at phase φ_4 for $T^+ = 250$; the coordinates of the maximum, marked with a cross, can be read on the axes. (*b*,*d*,*f*) Phase variation of their maxima in the (r_z^+, Y^+) plane, with a horizontal solid line indicating the value of the uncontrolled flow.

In contrast, $\pi_{22,m}^{s}$ and $\pi_{33,m}^{s}$ are minima at φ_2 and maxima at φ_4 (this is not inconsistent with the incompressibility constraint $\pi_{11}^{s} + \pi_{22}^{s} + \pi_{33}^{s} = 0$, since the three maxima occur at different scales and positions). As already mentioned in § 4.1.2, $\pi_{33,m}^{s}$ and $\overline{\delta w''\delta w''}_m$ have the same phase dependence, confirming that the tilting of the near-wall structures is accompanied by a redistribution of the streamwise fluctuations towards the spanwise ones.

4.4. *Transfers of the spanwise stresses*

A peculiarity of the present flow is the direct connection between the Stokes layer and the stochastic stresses, described by the coherent–stochastic production P_{11}^{cs} and P_{33}^{cs} shown in figure 3. It is therefore interesting to examine the variable-phase scale-space transfers of the stochastic stresses by looking at their fluxes in the scale and physical spaces. In this analysis, we only consider the transfer of spanwise stresses $\overline{\delta w''\delta w''}$, since for the streamwise stresses p_{11}^{cs} is negligible compared with p_{11}^{ms}. Moreover, only the $T^+ = 250$ case is considered, as the one where the effect of the Stokes layer on the w'' field is larger. For simplicity, the analysis is restricted to the $r_x = r_y = 0$ subspace, where the budget of $\overline{\delta w''\delta w''}$ can be rewritten by moving to the right-hand side the off-plane flux divergence

terms $\partial\phi^s_{x,33}/\partial r_x$, $\partial\phi^s_{y,33}/\partial r_y$ and the phase evolution term, as follows:

$$\frac{\partial\phi^s_{z,33}}{\partial r_z}+\frac{\partial\psi^s_{33}}{\partial Y}=\underbrace{p^{cs}_{33}+\pi^s_{33}+d^s_{33}}_{\xi^s_{33}}-\frac{\partial\phi^s_{x,33}}{\partial r_x}-\frac{\partial\phi^s_{y,33}}{\partial r_y}-\omega\frac{\partial\overline{\delta w''\delta w''}}{\partial\varphi}. \tag{4.5}$$

In this way, the left-hand side features the divergence of the in-plane flux vector, which provides information on the energetic relevance of the fluxes with its intensity, and shows their direction via its field lines. Moreover, the off-plane fluxes (i.e. the last three terms in the equation above) are always very small, and the in-plane divergence approximates well the full source term ξ^s_{33} everywhere (Gatti *et al.* 2020). This descends from a combination of the symmetries of the plane channel flow system and of the approximate alignment of the dominant vortical structures with the streamwise direction. Hence, the scale-space properties of the source term ξ^s_{33} approximate well those of the divergence of the in-plane flux.

Figure 13 plots the map of $\xi^s_{33}=p^{cs}_{33}+\pi^s_{33}+d^s_{33}$ for the uncontrolled case (where $p^{cs}_{33}=0$) and the controlled case at $T^+=250$ for φ_1, φ_2, φ_3 and φ_4, with the field lines of the in-plane flux coloured with its divergence. In the uncontrolled case, a region with $\xi^s_{33}>0$ extends for $5\lessapprox Y^+\lessapprox 100$ and for $r^+_z\gtrapprox 15$, at scales and positions where the pressure–strain dominates over dissipation. When control is active, instead, ξ^s_{33} receives the additional contribution from coherent–stochastic production, and the values of ξ^s_{33} are generally larger. Two regions with $\xi^s_{33}>0$ exist. One is close to the wall at $Y^+\approx 10$–20, and extends for all scales $r^+_z\gtrapprox 15$, with a peak at $r^+_z\approx 40$. A second, connected region involves larger wall distances and scales, in the $40\lessapprox r^+_z\lessapprox 200$ range. It is clearly visible in figure 14, where the ratio $\pi^s_{33}/(\xi^s_{33}-d^s_{33})$ is plotted to determine the main contribution to these positive sources at the different phases. When $\pi^s_{33}/(\xi^s_{33}-d^s_{33})>0.5$, $\pi^s_{33}>p^{cs}_{33}$ meaning that the pressure–strain is the largest contribution to the positive source. When $\pi^s_{33}/(\xi^s_{33}-d^s_{33})<0.5$, instead, the main contributor is the coherent–stochastic production p^{cs}_{33}. Figure 14 shows that p^{cs}_{33} and π^s_{33} both contribute to the near-wall source, but their relative importance changes with the phase. For φ_2 and φ_3, p^{cs}_{33} is the main contributor to the intense source peak. For φ_1 and φ_4, instead, p^{cs}_{33} weakens (see figure 11): now the (weaker) source is mainly fed by the pressure–strain. The source at larger Y, instead, is dominated by the pressure–strain at all phases; this is reasonable, as for $y^+>30$ the Stokes layer and consequently the coherent–stochastic production are weak.

As for the sinks, figure 13 shows three of them: viscous effects dominate the very near-wall region ($Y\to 0$), the bulk flow ($Y\to h$) and the smallest scales ($r_z\to 0$). Extension and intensity of these sinks change with φ, according to the evolution of p^{cs}_{33}, π^s_{33} and d^s_{33}. A cut-off scale $r_{z,min}$ (Chiarini *et al.* 2022*a*) can also be plotted to quantify the minimal scale where (spanwise) energy is always dissipated, regardless of the wall distance.

The field lines of $\overline{\delta w''\delta w''}$ drawn in figure 13 originate from a singularity point, i.e. a point near the source peak where the direction of the fluxes is undefined. Here the lines are energised by the intense positive source and transfer $\overline{\delta w''\delta w''}$ towards the sinks. Three types of lines are recognised, depending on where they vanish, and reflect the three sinks described above. Overall, these fluxes indicate the coexistence of ascending/descending and direct/inverse energy transfers, as described by Cimarelli *et al.* (2013, 2016) and Chiarini *et al.* (2022*b*) in the context of Poiseuille and Couette turbulent flows.

The three line types possess the same topology in the uncontrolled and controlled cases. For the latter, though, the amount of spanwise energy withdrawn from the sources and

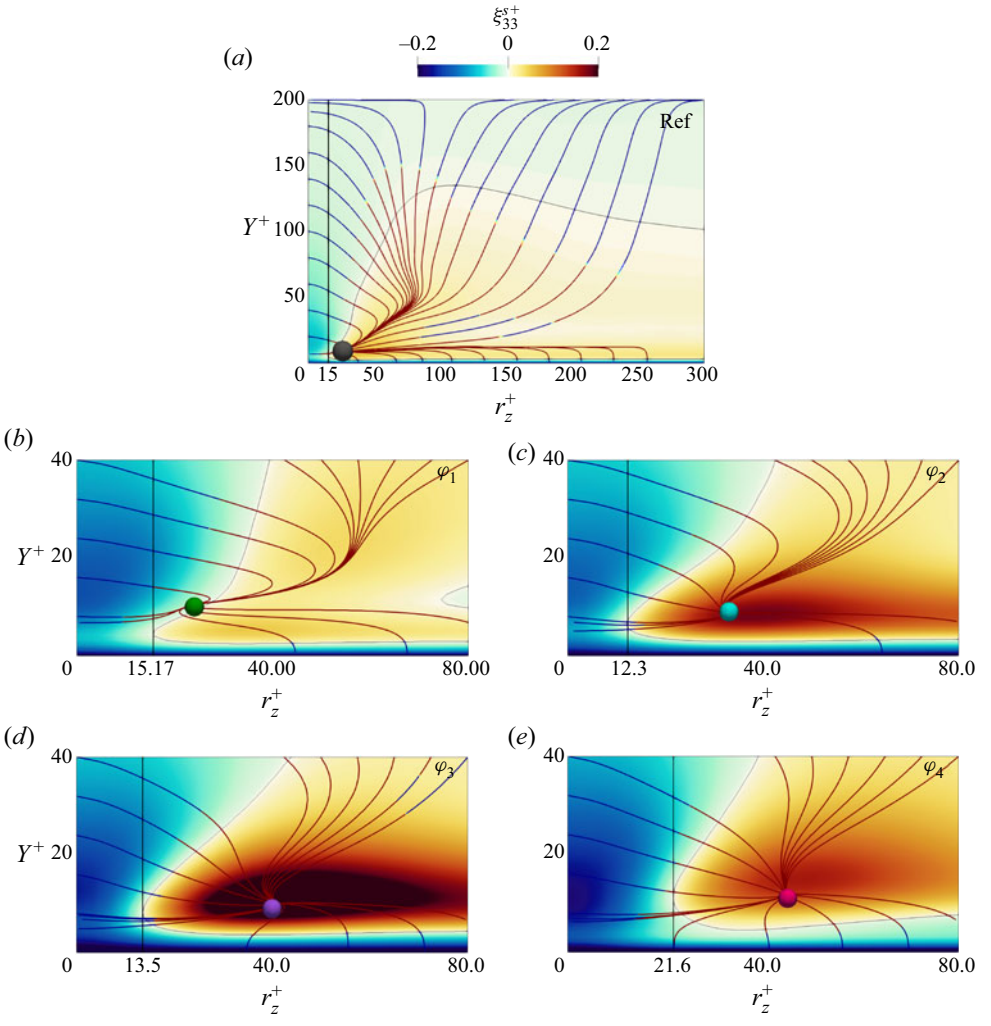

Figure 13. Source ξ_{33}^{s+} in the (r_z^+, Y^+) plane, with field lines of the in-plane flux vector coloured with its divergence for (*a*) the uncontrolled case and for the controlled case at $T^+ = 250$ at phases (*b*) φ_1, (*c*) φ_2, (*d*) φ_3 and (*e*) φ_4. The thin contour line marks the zero level. Dots (coloured according to figure 2) indicate the singularity point for the near-wall source, and the black vertical line marks the cut-off spanwise scale $r_{z,min}^+$ (see text).

released to the sinks changes with φ. An estimate of this change is provided by the phase evolution of the positive peak of the two-dimensional divergence of the flux vector. Its value is maximum at φ_3 where it is 3.36, 1.56 and 1.29 times larger than at φ_1, φ_2 and φ_4, respectively. This is consistent with the phase evolution of the positive peak of p_{33}^{cs} visualised in figure 11. Moreover, the singularity point lies in the source region dominated by p_{33}^{cs}, and its r_z position moves with φ following the peak of p_{33}^{cs}, being $r_z^+ = 24$, 33, 40 and 45 for φ_1, φ_2, φ_3 and φ_4; for the uncontrolled case it is $r_z^+ = 26$.

We therefore conclude that, at least for the $T^+ = 250$ case discussed here, the phase dependence of the transfers of $\overline{\delta w'' \delta w''}$ is governed by the p_{33}^{cs} contribution to ξ_{33}^{s} rather than by π_{33}^{s}. At all phases, the largest part of $\overline{\delta w'' \delta w''}$ withdrawn by the source is released in the near-wall region; a relatively smaller part goes to the smallest scales, and a minimal

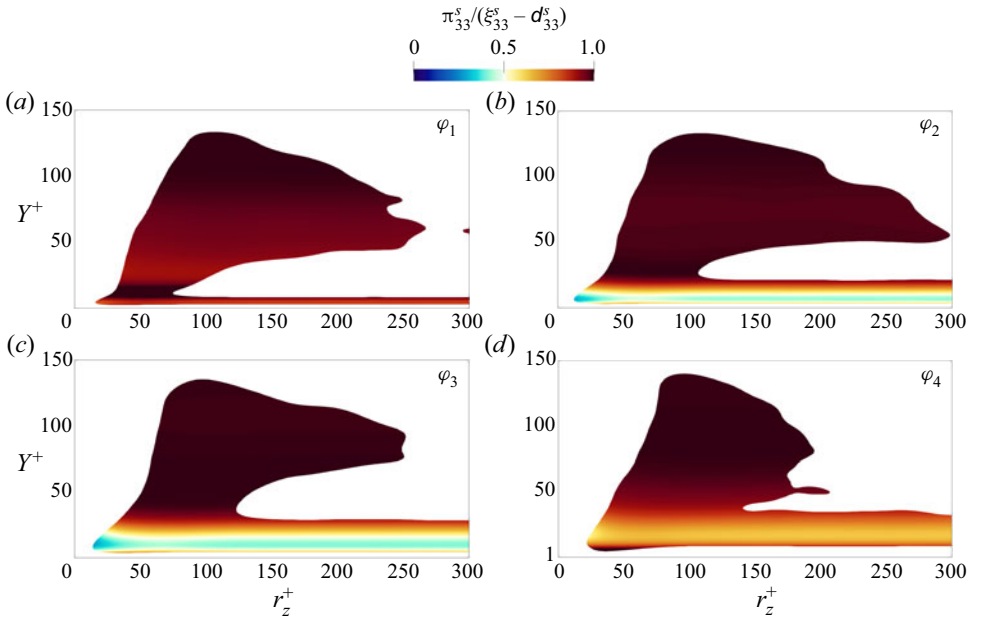

Figure 14. Region with positive source in the (r_z^+, Y^+) plane at phases (*a*) φ_1, (*b*) φ_2, (*c*) φ_3 and (*d*) φ_4 for $T^+ = 250$. The colour scale is for the ratio $\pi^s_{33}/(\xi^s_{33} - d^s_{33})$ and is centred at 0.5: red means $\pi^s_{33} > p^{cs}_{33}$ and blue means $\pi^s_{33} < p^{cs}_{33}$.

part goes towards the channel centre, where the turbulent activity is low. By comparing the negative peaks of the divergence of the in-plane flux vector at the wall and at the smallest scales, it is established that in the uncontrolled case the amount of $\overline{\delta w'' \delta w''}$ released at $Y \to 0$ is 5.67 times larger than that released at $r_z \to 0$. The oscillating wall alters the relative importance of the fluxes: the amount of $\overline{\delta w'' \delta w''}$ released at $Y \to 0$ is significantly less, being 2.62, 3.85, 2.46 and 2.41 times larger than that released at $r_z \to 0$ at phases φ_1, φ_2, φ_3 and φ_4, respectively.

5. Concluding discussion

We have derived the φAGKE, inferred from the incompressible Navier–Stokes equations, after a triple decomposition to separate the velocity and pressure fields into their coherent and stochastic parts.

The φAGKE are exact budget equations for the coherent and stochastic contributions to the second-order structure function tensor, namely $\delta\tilde{u}_i\delta\tilde{u}_j(\boldsymbol{X}, \boldsymbol{r}, \varphi)$ and $\overline{\delta u_i'' \delta u_j''}(\boldsymbol{X}, \boldsymbol{r}, \varphi)$. Compared with the standard AGKE, which are based on the classic (double) Reynolds decomposition, the φAGKE add extra features. (i) The transport equations for the coherent and stochastic parts are separated: disentangling their dynamics becomes possible. (ii) The scale-space energy exchanges among mean, coherent and stochastic fields can be tracked. In particular, the mean–coherent production p^{mc}_{ij} and the mean–stochastic production p^{ms}_{ij} bring out scales and positions where the mean flow feeds, and/or drains energy from, the coherent and stochastic fields; the coherent–stochastic production p^{cs}_{ij} describes the exchange between the coherent and stochastic fields. (iii) An extra term in the budget for $\delta\tilde{u}_i\delta\tilde{u}_j$ represents the mutual interaction of the coherent motions at different phases. (iv) The φAGKE imply no average over phases, and thus describe the phase variation of the

various terms related to coherent and stochastic motions. Once a phase average is taken, as in Alves Portela *et al.* (2020), phase information is obviously lost.

To demonstrate the potential of the φAGKE, we have applied them to a turbulent plane channel flow in which spanwise wall oscillations reduce the turbulent skin friction. The φAGKE are perfectly suited for this flow, owing to its deterministic and periodic external forcing; moreover, the physics of drag reduction remains not entirely understood and contains interesting interphase and multiscale dynamics.

Thanks to the φAGKE, the phase-dependent modifications of the near-wall turbulent structures have been observed without the need for somewhat arbitrary procedures to educe phase-locked and conditionally averaged structures. The flow scales involved in the redistribution of fluctuating energy have been described, together with the process by which streamwise velocity fluctuations are converted into spanwise ones by the action of pressure–strain. The interaction among the mean, coherent and stochastic fields is easily observed with the φAGKE, which highlight the energy exchanges between the coherent and stochastic fields, driven by the interaction between the quasi-streamwise vortices and the coherent spanwise shear. The phase-by-phase, scale-space transfers of the spanwise stochastic stresses, observed here for the first time, have revealed a significant phase dependency for the spanwise energy fluxes, which present ascending/descending and direct/inverse energy transfers at all phases.

The φAGKE can be leveraged to arrive at a thorough description of two-point second-order statistics in cases that reach far beyond the oscillating-wall problem, used here as a representative example only. Turbulent flows where an external periodic forcing is present are common: oscillating airfoils, rotors and turbines are only a few examples. Moreover, the φAGKE can also be used to tackle turbulent flows without a strictly periodic forcing, in which stochastic fluctuations coexist with some kind of coherent motion. A non-exhaustive list includes the turbulent flow past bluff bodies, where large-scale motions typical of the Kármán-like vortices in the wake coexist with the stochastic motion of smaller scale (Provansal, Mathis & Boyer 1987); the Taylor–Couette flow, in which Taylor–Görtler vortices develop and remain visible well into the turbulent regime (Koschmieder 1979); and the atmospheric boundary layer, rich with quasi-two-dimensional structures forced at smaller scales (Young *et al.* 2002). In such cases, though, the period of the oscillation is not uniquely identified, and attention has to be paid to properly define a phase reference.

Lastly, it should be realised that the specific triple decomposition behind the φAGKE does not matter: alternatives to the temporal triple decomposition could be used with a different meaning attached to the $\tilde{\cdot}$ and $\cdot''$ operators, without altering the ensuing equations. One example is the spatial triple decomposition approach adopted for example by Bech & Andersson (1996) and Gai *et al.* (2016) to decompose the velocity fluctuations into secondary flow and residual fluctuations in a rotating turbulent plane Couette flow. A further use case for the φAGKE would be a turbulent flow over a flat wall with a periodic pattern, e.g. riblets or dimples, in which the phase average would be again spatially defined. Finally, another option is to employ a scale-based triple decomposition. For example, Andreolli, Quadrio & Gatti (2021) used a scale decomposition mutated from Kawata & Alfredsson (2018) to separate the fluctuating velocity field in a Couette flow into small- and large-scale components, examining the kinetic energy budget of both components in physical space. This information, compacted by Andreolli *et al.* (2021) through spatial integration into an energy budget without independent variables, similar to that in figure 3, can instead be expanded at will in the full physical and scale space thanks to the φAGKE, thus providing the ultimate information approximately two-point second-order statistics of the flow.

Declaration of interests. The authors report no conflict of interest.

Author ORCIDs.
Federica Gattere https://orcid.org/0000-0002-1450-415X;
Alessandro Chiarini https://orcid.org/0000-0001-7746-2850;
Emanuele Gallorini https://orcid.org/0000-0002-8547-3100;
Maurizio Quadrio https://orcid.org/0000-0002-7662-3576.

Appendix A. Derivation of the budget equations for $\delta\tilde{u}_i\delta\tilde{u}_j$ and $\overline{\delta u_i''\delta u_j''}$

The derivation of the φAGKE via triple decomposition is described below, by listing the sequence of the main analytical steps.

A.1. *Budget equation for U_i, $\tilde{u}_i$ and u_i''*

The starting point is the incompressible Navier–Stokes equations:

$$\frac{\partial u_i}{\partial t} + u_k\frac{\partial u_i}{\partial x_k} = -\frac{1}{\rho}\frac{\partial p}{\partial x_i} + \nu\frac{\partial^2 u_i}{\partial x_k\partial x_k} + f_i. \tag{A1}$$

The triple decomposition (2.1) for u_i, p and f_i is introduced to obtain

$$\begin{aligned}\frac{\partial\tilde{u}_i}{\partial t} + \frac{\partial u_i''}{\partial t} + \left(U_k + \tilde{u}_k + u_k''\right)\frac{\partial}{\partial x_k}\left(U_i + \tilde{u}_i + u_i''\right) &= -\frac{1}{\rho}\frac{\partial}{\partial x_i}\left(P + \tilde{p} + p''\right)\\ &+ \nu\frac{\partial^2}{\partial x_k\partial x_k}\left(U_i + \tilde{u}_i + u_i''\right) + F_i + \tilde{f}_i + f_i'',\end{aligned} \tag{A2}$$

which can be reorganised as

$$\begin{aligned}&\frac{\partial\tilde{u}_i}{\partial t} + \frac{\partial u_i''}{\partial t} + U_k\frac{\partial U_i}{\partial x_k} + U_k\frac{\partial\tilde{u}_i}{\partial x_k} + U_k\frac{\partial u_i''}{\partial x_k} + \tilde{u}_k\frac{\partial U_i}{\partial x_k} + \tilde{u}_k\frac{\partial\tilde{u}_i}{\partial x_k} + \tilde{u}_k\frac{\partial u_i''}{\partial x_k}\\ &\quad + u_k''\frac{\partial U_i}{\partial x_k} + u_k''\frac{\partial\tilde{u}_i}{\partial x_k} + u_k''\frac{\partial u_i''}{\partial x_k} = -\frac{1}{\rho}\frac{\partial P}{\partial x_i} - \frac{1}{\rho}\frac{\partial\tilde{p}}{\partial x_i} - \frac{1}{\rho}\frac{\partial p''}{\partial x_i}\\ &\quad + \nu\frac{\partial^2 U_i}{\partial x_k\partial x_k} + \nu\frac{\partial^2\tilde{u}_i}{\partial x_k\partial x_k} + \nu\frac{\partial^2 u_i''}{\partial x_k\partial x_k} + F_i + \tilde{f}_i + f_i''.\end{aligned} \tag{A3}$$

Now the averaging operator $\langle\cdot\rangle$ is used to arrive at the budget equation for U_i, i.e.

$$U_k\frac{\partial U_i}{\partial x_k} + \left\langle\tilde{u}_k\frac{\partial\tilde{u}_i}{\partial x_k}\right\rangle + \left\langle u_k''\frac{\partial u_i''}{\partial x_k}\right\rangle = -\frac{1}{\rho}\frac{\partial P}{\partial x_i} + \nu\frac{\partial^2 U_i}{\partial x_k\partial x_k} + F_i. \tag{A4}$$

When, instead, the phase average operator $\bar{\cdot}$ is used, we get

$$\begin{aligned}&\frac{\partial\tilde{u}_i}{\partial t} + U_k\frac{\partial U_i}{\partial x_k} + \tilde{u}_k\frac{\partial U_i}{\partial x_k} + U_k\frac{\partial\tilde{u}_i}{\partial x_k} + \tilde{u}_k\frac{\partial\tilde{u}_i}{\partial x_k} + \overline{u_k''\frac{\partial u_i''}{\partial x_k}}\\ &\quad = -\frac{1}{\rho}\frac{\partial P}{\partial x_i} - \frac{1}{\rho}\frac{\partial\tilde{p}}{\partial x_i} + \nu\frac{\partial^2 U_i}{\partial x_k\partial x_k} + \nu\frac{\partial^2\tilde{u}_i}{\partial x_k\partial x_k} + F_i + \tilde{f}_i,\end{aligned} \tag{A5}$$

which can be written differently using the budget equation for U_i, i.e.

$$\frac{\partial \tilde{u}_i}{\partial t} + \tilde{u}_k \frac{\partial U_i}{\partial x_k} + U_k \frac{\partial \tilde{u}_i}{\partial x_k} + \tilde{u}_k \frac{\partial \tilde{u}_i}{\partial x_k} + \overline{u_k'' \frac{\partial u_i''}{\partial x_k}} - \left\langle \tilde{u}_k \frac{\partial \tilde{u}_i}{\partial x_k} \right\rangle - \left\langle u_k'' \frac{\partial u_i''}{\partial x_k} \right\rangle = -\frac{1}{\rho} \frac{\partial \tilde{p}}{\partial x_i} + \nu \frac{\partial^2 \tilde{u}_i}{\partial x_k \partial x_k} + \tilde{f}_i. \tag{A6}$$

This leads to the budget equation for $\tilde{u}_i$, i.e.

$$\frac{\partial \tilde{u}_i}{\partial t} + U_k \frac{\partial \tilde{u}_i}{\partial x_k} + \tilde{u}_k \frac{\partial U_i}{\partial x_k} + \frac{\partial}{\partial x_k} \left(\tilde{u}_i \tilde{u}_k - \langle \tilde{u}_i \tilde{u}_k \rangle \right) + \frac{\partial}{\partial x_k} \left(\overline{u_i'' u_k''} - \langle u_i'' u_k'' \rangle \right) = -\frac{1}{\rho} \frac{\partial \tilde{p}}{\partial x_i} + \nu \frac{\partial^2 \tilde{u}_i}{\partial x_k \partial x_k} + \tilde{f}_i. \tag{A7}$$

The budget equation for u_i'' is obtained by subtracting from (A3) the budget equations for U_i (A4) and $\tilde{u}_i$ (A7):

$$\frac{\partial u_i''}{\partial t} + U_k \frac{\partial u_i''}{\partial x_k} + \tilde{u}_k \frac{\partial u_i''}{\partial x_k} + u_k'' \frac{\partial U_i}{\partial x_k} + u_k'' \frac{\partial \tilde{u}_i}{\partial x_k} + \frac{\partial}{\partial x_k} \left(u_i'' u_k'' - \overline{u_i'' u_k''} \right) = -\frac{1}{\rho} \frac{\partial p''}{\partial x_i} + \nu \frac{\partial^2 u_i''}{\partial x_k \partial x_k} + f_i''. \tag{A8}$$

A.2. *The φAGKE for $\delta\tilde{u}_i\delta\tilde{u}_j$*

The budget equation for $\tilde{u}_i$ in $\boldsymbol{x}$ is subtracted from that evaluated in $\boldsymbol{x}^+ = \boldsymbol{x} + \boldsymbol{r}$:

$$\delta\left(\frac{\partial \tilde{u}_i}{\partial t}\right) + \delta\left(U_k \frac{\partial \tilde{u}_i}{\partial x_k}\right) + \delta\left(\tilde{u}_k \frac{\partial U_i}{\partial x_k}\right) + \delta\left(\frac{\partial}{\partial x_k}\left(\tilde{u}_i \tilde{u}_k - \langle \tilde{u}_i \tilde{u}_k \rangle\right)\right) + \delta\left(\frac{\partial}{\partial x_k}\left(\overline{u_i'' u_k''} - \langle u_i'' u_k'' \rangle\right)\right) = -\delta\left(\frac{1}{\rho}\frac{\partial \tilde{p}}{\partial x_i}\right) + \delta\left(\nu \frac{\partial^2 \tilde{u}_i}{\partial x_k \partial x_k}\right) + \delta\left(\tilde{f}_i\right). \tag{A9}$$

By recalling that the two reference systems are independent, one may write for example

$$\delta\left(U_k \frac{\partial \tilde{u}_i}{\partial x_k}\right) = U_k^+ \frac{\partial \delta\tilde{u}_i}{\partial x_k^+} + U_k \frac{\partial \delta\tilde{u}_i}{\partial x_k}; \tag{A10}$$

using the same line of reasoning for all the other terms one obtains

$$\frac{\partial \delta\tilde{u}_i}{\partial t} + U_k^+ \frac{\partial \delta\tilde{u}_i}{\partial x_k^+} + U_k \frac{\partial \delta\tilde{u}_i}{\partial x_k} + \tilde{u}_k^+ \frac{\partial \delta U_i}{\partial x_k^+} + \tilde{u}_k \frac{\partial \delta U_i}{\partial x_k} + \tilde{u}_k^+ \frac{\partial \delta\tilde{u}_i}{\partial x_k^+} + \tilde{u}_k \frac{\partial \delta\tilde{u}_i}{\partial x_k} - \left\langle \tilde{u}_k^+ \frac{\partial \delta\tilde{u}_i}{\partial x_k^+} \right\rangle - \left\langle \tilde{u}_k \frac{\partial \delta\tilde{u}_i}{\partial x_k} \right\rangle + \overline{u_k''^+ \frac{\partial \delta u_i''}{\partial x_k^+}} + \overline{u_k'' \frac{\partial \delta u_i''}{\partial x_k}} - \left\langle u_k''^+ \frac{\partial \delta u_i''}{\partial x_k^+} \right\rangle - \left\langle u_k'' \frac{\partial \delta u_i''}{\partial x_k} \right\rangle = -\frac{1}{\rho}\frac{\partial \delta\tilde{p}}{\partial x_i^+} - \frac{1}{\rho}\frac{\partial \delta\tilde{p}}{\partial x_i} + \nu\left(\frac{\partial^2}{\partial x_k^+ \partial x_k^+} + \frac{\partial^2}{\partial x_k \partial x_k}\right)\delta\tilde{u}_i + \delta\tilde{f}_i. \tag{A11}$$

Then one may write for example

$$\tilde{u}_k^+ \frac{\partial \delta\tilde{u}_i}{\partial x_k^+} = \delta\tilde{u}_k \frac{\partial \delta\tilde{u}_i}{\partial x_k^+} + \tilde{u}_k \frac{\partial \delta\tilde{u}_i}{\partial x_k^+} \tag{A12}$$

and using this expression for all the terms we obtain the budget equation for $\delta\tilde{u}_i$:

$$\begin{aligned}
&\frac{\partial \delta\tilde{u}_i}{\partial t} + \delta U_k \frac{\partial \delta\tilde{u}_i}{\partial x_k^+} + U_k \left(\frac{\partial}{\partial x_k^+} + \frac{\partial}{\partial x_k} \right) \delta\tilde{u}_i + \delta\tilde{u}_k \frac{\partial \delta U_i}{\partial x_k^+} + \tilde{u}_k \left(\frac{\partial}{\partial x_k^+} + \frac{\partial}{\partial x_k} \right) \delta U_i \\
&\quad + \delta\tilde{u}_k \frac{\partial \delta\tilde{u}_i}{\partial x_k^+} + \tilde{u}_k \left(\frac{\partial}{\partial x_k^+} + \frac{\partial}{\partial x_k} \right) \delta\tilde{u}_i - \left\langle \delta\tilde{u}_k \frac{\partial \delta\tilde{u}_i}{\partial x_k^+} \right\rangle - \left\langle \tilde{u}_k \left(\frac{\partial}{\partial x_k^+} + \frac{\partial}{\partial x_k} \right) \delta\tilde{u}_i \right\rangle \\
&\quad + \overline{\delta u_k'' \frac{\partial \delta u_i''}{\partial x_k^+}} + \overline{u_k'' \left(\frac{\partial}{\partial x_k^+} + \frac{\partial}{\partial x_k} \right) \delta u_i''} - \left\langle \delta u_k'' \frac{\partial \delta u_i''}{\partial x_k^+} \right\rangle - \left\langle u_k'' \left(\frac{\partial}{\partial x_k^+} + \frac{\partial}{\partial x_k} \right) \delta u_i'' \right\rangle \\
&= -\frac{1}{\rho} \frac{\partial \delta\tilde{p}}{\partial x_i^+} - \frac{1}{\rho} \frac{\partial \delta\tilde{p}}{\partial x_i} + \nu \left(\frac{\partial^2}{\partial x_k^+ \partial x_k^+} + \frac{\partial^2}{\partial x_k \partial x_k} \right) \delta\tilde{u}_i + \delta\tilde{f}_i.
\end{aligned} \tag{A13}$$

This equation is multiplied by $\delta\tilde{u}_j$ to obtain

$$\begin{aligned}
&\delta\tilde{u}_j \frac{\partial \delta\tilde{u}_i}{\partial t} + \delta\tilde{u}_j \delta U_k \frac{\partial \delta\tilde{u}_i}{\partial x_k^+} + \delta\tilde{u}_j U_k \left(\frac{\partial}{\partial x_k^+} + \frac{\partial}{\partial x_k} \right) \delta\tilde{u}_i + \delta\tilde{u}_j \delta\tilde{u}_k \frac{\partial \delta U_i}{\partial x_k^+} \\
&\quad + \delta\tilde{u}_j \tilde{u}_k \left(\frac{\partial}{\partial x_k^+} + \frac{\partial}{\partial x_k} \right) \delta U_i + \delta\tilde{u}_j \delta\tilde{u}_k \frac{\partial \delta\tilde{u}_i}{\partial x_k^+} + \delta\tilde{u}_j \tilde{u}_k \left(\frac{\partial}{\partial x_k^+} + \frac{\partial}{\partial x_k} \right) \delta\tilde{u}_i - \delta\tilde{u}_j \left\langle \delta\tilde{u}_k \frac{\partial \delta\tilde{u}_i}{\partial x_k^+} \right\rangle \\
&\quad - \delta\tilde{u}_j \left\langle \tilde{u}_k \left(\frac{\partial}{\partial x_k^+} + \frac{\partial}{\partial x_k} \right) \delta\tilde{u}_i \right\rangle + \delta\tilde{u}_j \overline{\delta u_k'' \frac{\partial \delta u_i''}{\partial x_k^+}} + \delta\tilde{u}_j \overline{u_k'' \left(\frac{\partial}{\partial x_k^+} + \frac{\partial}{\partial x_k} \right) \delta u_i''} \\
&\quad - \delta\tilde{u}_j \left\langle \delta u_k'' \frac{\partial \delta u_i''}{\partial x_k^+} \right\rangle - \delta\tilde{u}_j \left\langle u_k'' \left(\frac{\partial}{\partial x_k^+} + \frac{\partial}{\partial x_k} \right) \delta u_i'' \right\rangle = -\delta\tilde{u}_j \frac{1}{\rho} \left(\frac{\partial}{\partial x_i^+} + \frac{\partial}{\partial x_i} \right) \delta\tilde{p} \\
&\quad + \nu \delta\tilde{u}_j \left(\frac{\partial^2}{\partial x_k^+ \partial x_k^+} + \frac{\partial^2}{\partial x_k \partial x_k} \right) \delta\tilde{u}_i + \delta\tilde{u}_j \delta\tilde{f}_i.
\end{aligned} \tag{A14}$$

The same equation is written again by swapping the i and j indices, and the two equations are then summed together:

$$\begin{aligned}
&\frac{\partial}{\partial t} \delta\tilde{u}_i \delta\tilde{u}_j + \delta\tilde{u}_j \delta U_k \frac{\partial \delta\tilde{u}_i}{\partial x_k^+} + \delta\tilde{u}_i \delta U_k \frac{\partial \delta\tilde{u}_j}{\partial x_k^+} + \delta\tilde{u}_j U_k \left(\frac{\partial}{\partial x_k^+} + \frac{\partial}{\partial x_k} \right) \delta\tilde{u}_i \\
&\quad + \delta\tilde{u}_i U_k \left(\frac{\partial}{\partial x_k^+} + \frac{\partial}{\partial x_k} \right) \delta\tilde{u}_j + \delta\tilde{u}_j \delta\tilde{u}_k \frac{\partial \delta U_i}{\partial x_k^+} + \delta\tilde{u}_i \delta\tilde{u}_k \frac{\partial \delta U_j}{\partial x_k^+} + \delta\tilde{u}_j \tilde{u}_k \left(\frac{\partial}{\partial x_k^+} + \frac{\partial}{\partial x_k} \right) \delta U_i \\
&\quad + \delta\tilde{u}_i \tilde{u}_k \left(\frac{\partial}{\partial x_k^+} + \frac{\partial}{\partial x_k} \right) \delta U_j + \delta\tilde{u}_j \delta\tilde{u}_k \frac{\partial \delta\tilde{u}_i}{\partial x_k^+} + \delta\tilde{u}_i \delta\tilde{u}_k \frac{\partial \delta\tilde{u}_j}{\partial x_k^+} + \delta\tilde{u}_j \tilde{u}_k \left(\frac{\partial}{\partial x_k^+} + \frac{\partial}{\partial x_k} \right) \delta\tilde{u}_i
\end{aligned}$$

$$
\begin{aligned}
&+ \delta\tilde{u}_i\tilde{u}_k\left(\frac{\partial}{\partial x_k^+}+\frac{\partial}{\partial x_k}\right)\delta\tilde{u}_j - \delta\tilde{u}_j\left\langle\delta\tilde{u}_k\frac{\partial\delta\tilde{u}_i}{\partial x_k^+}\right\rangle - \delta\tilde{u}_i\left\langle\delta\tilde{u}_k\frac{\partial\delta\tilde{u}_j}{\partial x_k^+}\right\rangle\\
&- \delta\tilde{u}_j\left\langle\tilde{u}_k\left(\frac{\partial}{\partial x_k^+}+\frac{\partial}{\partial x_k}\right)\delta\tilde{u}_i\right\rangle - \delta\tilde{u}_i\left\langle\tilde{u}_k\left(\frac{\partial}{\partial x_k^+}+\frac{\partial}{\partial x_k}\right)\delta\tilde{u}_j\right\rangle\\
&+ \delta\tilde{u}_j\overline{\delta u_k''\frac{\partial\delta u_i''}{\partial x_k^+}} + \delta\tilde{u}_i\overline{\delta u_k''\frac{\partial\delta u_j''}{\partial x_k^+}} + \delta\tilde{u}_j\overline{u_k''\left(\frac{\partial}{\partial x_k^+}+\frac{\partial}{\partial x_k}\right)\delta u_i''}\\
&+ \delta\tilde{u}_i\overline{u_k''\left(\frac{\partial}{\partial x_k^+}+\frac{\partial}{\partial x_k}\right)\delta u_j''} - \delta\tilde{u}_j\left\langle\delta u_k''\frac{\partial\delta u_i''}{\partial x_k^+}\right\rangle - \delta\tilde{u}_j\left\langle u_k''\left(\frac{\partial}{\partial x_k^+}+\frac{\partial}{\partial x_k}\right)\delta u_i''\right\rangle\\
&- \delta\tilde{u}_i\left\langle\delta u_k''\frac{\partial\delta u_j''}{\partial x_k^+}\right\rangle - \delta\tilde{u}_i\left\langle u_k''\left(\frac{\partial}{\partial x_k^+}+\frac{\partial}{\partial x_k}\right)\delta u_j''\right\rangle = -\delta\tilde{u}_j\frac{1}{\rho}\left(\frac{\partial}{\partial x_i^+}+\frac{\partial}{\partial x_i}\right)\delta\tilde{p}\\
&- \delta\tilde{u}_i\frac{1}{\rho}\left(\frac{\partial}{\partial x_j^+}+\frac{\partial}{\partial x_j}\right)\delta\tilde{p} + \nu\delta\tilde{u}_j\left(\frac{\partial^2}{\partial x_k^+\partial x_k^+}+\frac{\partial^2}{\partial x_k\partial x_k}\right)\delta\tilde{u}_i\\
&+ \nu\delta\tilde{u}_i\left(\frac{\partial^2}{\partial x_k^+\partial x_k^+}+\frac{\partial^2}{\partial x_k\partial x_k}\right)\delta\tilde{u}_j + \delta\tilde{u}_j\delta\tilde{f}_i + \delta\tilde{u}_i\delta\tilde{f}_j. \qquad \text{(A15)}
\end{aligned}
$$

At this point, after applying the phase average operator $\bar{\cdot}$ and manipulating the equations, one obtains

$$
\begin{aligned}
&\frac{\partial}{\partial t}\delta\tilde{u}_i\delta\tilde{u}_j + \frac{\partial}{\partial x_k^+}\delta U_k\delta\tilde{u}_i\delta\tilde{u}_j + \left(\frac{\partial}{\partial x_k^+}+\frac{\partial}{\partial x_k}\right)U_k\delta\tilde{u}_i\delta\tilde{u}_j + \delta\tilde{u}_j\delta\tilde{u}_k\frac{\partial\delta U_i}{\partial x_k^+} + \delta\tilde{u}_i\delta\tilde{u}_k\frac{\partial\delta U_j}{\partial x_k^+}\\
&\quad+ \delta\tilde{u}_j\tilde{u}_k\left(\frac{\partial}{\partial x_k^+}+\frac{\partial}{\partial x_k}\right)\delta U_i + \delta\tilde{u}_i\tilde{u}_k\left(\frac{\partial}{\partial x_k^+}+\frac{\partial}{\partial x_k}\right)\delta U_j + \frac{\partial}{\partial x_k^+}\delta\tilde{u}_k\delta\tilde{u}_i\delta\tilde{u}_j\\
&\quad+ \left(\frac{\partial}{\partial x_k^+}+\frac{\partial}{\partial x_k}\right)\tilde{u}_k\delta\tilde{u}_i\delta\tilde{u}_j - \delta\tilde{u}_j\left\langle\delta\tilde{u}_k\frac{\partial\delta\tilde{u}_i}{\partial x_k^+}\right\rangle - \delta\tilde{u}_i\left\langle\delta\tilde{u}_k\frac{\partial\delta\tilde{u}_j}{\partial x_k^+}\right\rangle\\
&\quad- \delta\tilde{u}_j\left\langle\tilde{u}_k\left(\frac{\partial}{\partial x_k^+}+\frac{\partial}{\partial x_k}\right)\delta\tilde{u}_i\right\rangle - \delta\tilde{u}_i\left\langle\tilde{u}_k\left(\frac{\partial}{\partial x_k^+}+\frac{\partial}{\partial x_k}\right)\delta\tilde{u}_j\right\rangle\\
&\quad+ \delta\tilde{u}_j\frac{\partial}{\partial x_k^+}\overline{\delta u_i''\delta u_k''} + \delta\tilde{u}_i\frac{\partial}{\partial x_k^+}\overline{\delta u_j''\delta u_k''} + \delta\tilde{u}_j\overline{u_k''\left(\frac{\partial}{\partial x_k^+}+\frac{\partial}{\partial x_k}\right)\delta u_i''}\\
&\quad+ \delta\tilde{u}_i\overline{u_k''\left(\frac{\partial}{\partial x_k^+}+\frac{\partial}{\partial x_k}\right)\delta u_j''} - \delta\tilde{u}_j\left\langle\delta u_k''\frac{\partial\delta u_i''}{\partial x_k^+}\right\rangle - \delta\tilde{u}_j\left\langle u_k''\left(\frac{\partial}{\partial x_k^+}+\frac{\partial}{\partial x_k}\right)\delta u_i''\right\rangle\\
&\quad- \delta\tilde{u}_i\left\langle\delta u_k''\frac{\partial\delta u_j''}{\partial x_k^+}\right\rangle - \delta\tilde{u}_i\left\langle u_k''\left(\frac{\partial}{\partial x_k^+}+\frac{\partial}{\partial x_k}\right)\delta u_j''\right\rangle = -\delta\tilde{u}_j\frac{1}{\rho}\left(\frac{\partial}{\partial x_i^+}+\frac{\partial}{\partial x_i}\right)\delta\tilde{p}
\end{aligned}
$$

$$- \delta\tilde{u}_i \frac{1}{\rho}\left(\frac{\partial}{\partial x_j^+} + \frac{\partial}{\partial x_j}\right)\delta\tilde{p} + \nu\delta\tilde{u}_j\left(\frac{\partial^2}{\partial x_k^+ \partial x_k^+} + \frac{\partial^2}{\partial x_k \partial x_k}\right)\delta\tilde{u}_i$$
$$+ \nu\delta\tilde{u}_i\left(\frac{\partial^2}{\partial x_k^+ \partial x_k^+} + \frac{\partial^2}{\partial x_k \partial x_k}\right)\delta\tilde{u}_j + \delta\tilde{u}_j\delta\tilde{f}_i + \delta\tilde{u}_i\delta\tilde{f}_j. \tag{A16}$$

We now introduce the new independent variables $\boldsymbol{X}$ and $\boldsymbol{r}$ such that

$$X_i = \frac{x_i + x_i^+}{2} \quad r_i = x_i^+ - x_i. \tag{A17}$$

As a result the x_i and x_i^+ derivatives are related to the X_i and r_i derivatives by the following relations:

$$\frac{\partial}{\partial x_i} = \frac{1}{2}\frac{\partial}{\partial X_i} - \frac{\partial}{\partial r_i}; \quad \frac{\partial}{\partial x_i^+} = \frac{1}{2}\frac{\partial}{\partial X_i} + \frac{\partial}{\partial r_i};$$
$$\frac{\partial^2}{\partial x_k^+ \partial x_k^+} + \frac{\partial^2}{\partial x_k \partial x_k} = \frac{1}{2}\frac{\partial^2}{\partial X_k \partial X_k} + 2\frac{\partial^2}{\partial r_k \partial r_k}. \tag{A18a–c}$$

Equation (A16) becomes

$$\frac{\partial}{\partial t}\delta\tilde{u}_i\tilde{u}_j + \left(\frac{1}{2}\frac{\partial}{\partial X_k} + \frac{\partial}{\partial r_k}\right)\delta U_k\delta\tilde{u}_i\delta\tilde{u}_j + \frac{\partial}{\partial X_k}U_k\delta\tilde{u}_i\delta\tilde{u}_j + \delta\tilde{u}_j\delta\tilde{u}_k\left(\frac{1}{2}\frac{\partial}{\partial X_k} + \frac{\partial}{\partial r_k}\right)\delta U_i$$
$$+ \delta\tilde{u}_i\delta\tilde{u}_k\left(\frac{1}{2}\frac{\partial}{\partial X_k} + \frac{\partial}{\partial r_k}\right)\delta U_j + \delta\tilde{u}_j\tilde{u}_k\frac{\partial}{\partial X_k}\delta U_i + \delta\tilde{u}_i\tilde{u}_k\frac{\partial}{\partial X_k}\delta U_j$$
$$+ \left(\frac{1}{2}\frac{\partial}{\partial X_k} + \frac{\partial}{\partial r_k}\right)(\delta\tilde{u}_k\delta\tilde{u}_i\delta\tilde{u}_j) + \frac{\partial}{\partial X_k}(\tilde{u}_k\delta\tilde{u}_i\delta\tilde{u}_j) - \frac{\partial}{\partial r_k}\langle\delta\tilde{u}_i\delta\tilde{u}_k\rangle\,\delta\tilde{u}_j + \langle\delta\tilde{u}_i\delta\tilde{u}_k\rangle\frac{\partial\delta\tilde{u}_j}{\partial r_k}$$
$$- \frac{\partial}{\partial X_k}\langle\tilde{u}_k^*\delta\tilde{u}_i\rangle\delta\tilde{u}_j + \langle\tilde{u}_k^*\delta\tilde{u}_i\rangle\frac{\partial\delta\tilde{u}_j}{\partial X_k} - \frac{\partial}{\partial r_k}\langle\delta\tilde{u}_j\delta\tilde{u}_k\rangle\delta\tilde{u}_i + \langle\delta\tilde{u}_j\delta\tilde{u}_k\rangle\frac{\partial\delta\tilde{u}_i}{\partial r_k} - \frac{\partial}{\partial X_k}\langle\tilde{u}_k^*\delta\tilde{u}_j\rangle\delta\tilde{u}_i$$
$$+ \langle\tilde{u}_k^*\delta\tilde{u}_j\rangle\frac{\partial\delta\tilde{u}_i}{\partial X_k} + \delta\tilde{u}_j\left(\frac{1}{2}\frac{\partial}{\partial X_k} + \frac{\partial}{\partial r_k}\right)\overline{\delta u_i''\delta u_k''} + \delta\tilde{u}_i\left(\frac{1}{2}\frac{\partial}{\partial X_k} + \frac{\partial}{\partial r_k}\right)\overline{\delta u_j''\delta u_k''}$$
$$+ \overline{\delta\tilde{u}_j u_k''\frac{\partial}{\partial X_k}\delta u_i''} + \overline{\delta\tilde{u}_i u_k''\frac{\partial}{\partial X_k}\delta u_j''} - \frac{\partial}{\partial r_k}\langle\delta u_i''\delta u_k''\rangle\delta\tilde{u}_j + \langle\delta u_i''\delta u_k''\rangle\frac{\partial\delta\tilde{u}_j}{\partial r_k}$$
$$- \frac{\partial}{\partial X_k}\langle u_k''^*\delta u_i''\rangle\delta\tilde{u}_j + \langle u_k''^*\delta u_i''\rangle\frac{\partial\delta\tilde{u}_j}{\partial X_k} - \frac{\partial}{\partial r_k}\langle\delta u_j''\delta u_k''\rangle\delta\tilde{u}_i$$
$$+ \langle\delta u_j''\delta u_k''\rangle\frac{\partial\delta\tilde{u}_i}{\partial r_k} - \frac{\partial}{\partial X_k}\langle u_k''^*\delta u_j''\rangle\delta\tilde{u}_i + \langle u_k''^*\delta u_j''\rangle\frac{\partial\delta\tilde{u}_i}{\partial X_k}$$
$$= -\delta\tilde{u}_j\frac{1}{\rho}\left(\frac{\partial}{\partial X_i}\right)\delta\tilde{p} - \delta\tilde{u}_i\frac{1}{\rho}\left(\frac{\partial}{\partial X_j}\right)\delta\tilde{p} + \nu\delta\tilde{u}_j\left(\frac{1}{2}\frac{\partial^2}{\partial X_k\partial X_k} + 2\frac{\partial^2}{\partial r_k\partial r_k}\right)\delta\tilde{u}_i$$
$$+ \nu\delta\tilde{u}_i\left(\frac{1}{2}\frac{\partial^2}{\partial X_k\partial X_k} + 2\frac{\partial^2}{\partial r_k\partial r_k}\right)\delta\tilde{u}_j + \delta\tilde{u}_j\delta\tilde{f}_i + \delta\tilde{u}_i\delta\tilde{f}_j, \tag{A19}$$

where the asterisk $(\cdot)^*$ denotes the average of any quantity between $\boldsymbol{x}$ and $\boldsymbol{x}^+$. We also observe that

$$\begin{aligned}
&\delta\tilde{u}_j\left(\frac{1}{2}\frac{\partial}{\partial X_k}+\frac{\partial}{\partial r_k}\right)\overline{\delta u_i''\delta u_k''}+\delta\tilde{u}_j\overline{u_k''\frac{\partial}{\partial X_k}\delta u_i''}\\
&\quad=\delta\tilde{u}_j\left(\frac{1}{2}\frac{\partial}{\partial X_k}+\frac{\partial}{\partial r_k}\right)\overline{\delta u_i''\delta u_k''}+\delta\tilde{u}_j\frac{\partial}{\partial X_k}\overline{u_k''\delta u_i''}\\
&\quad=\delta\tilde{u}_j\frac{\partial}{\partial r_k}\overline{\delta u_i''\delta u_k''}+\delta\tilde{u}_j\frac{\partial}{\partial X_k}\overline{\frac{1}{2}\left(u_k''+u_k''^{+}\right)\delta u_i''}\\
&\quad=\frac{\partial}{\partial r_k}\overline{\delta u_i''\delta u_k''}\delta\tilde{u}_j-\overline{\delta u_i''\delta u_k''}\frac{\partial\delta\tilde{u}_j}{\partial r_k}+\frac{\partial}{\partial X_k}\overline{u_k''^{*}\delta u_i''}\delta\tilde{u}_j-\overline{u_k''^{*}\delta u_i''}\frac{\partial}{\partial X_k}\delta\tilde{u}_j.
\end{aligned}\tag{A20}$$

The viscous term can be simplified as

$$\begin{aligned}
&\nu\delta\tilde{u}_j\left(\frac{1}{2}\frac{\partial^2}{\partial X_k\partial X_k}+2\frac{\partial^2}{\partial r_k\partial r_k}\right)\delta\tilde{u}_i+\nu\delta\tilde{u}_i\left(\frac{1}{2}\frac{\partial^2}{\partial X_k\partial X_k}+2\frac{\partial^2}{\partial r_k\partial r_k}\right)\delta\tilde{u}_j\\
&\quad=\frac{\nu}{2}\frac{\partial^2}{\partial X_k\partial X_k}\delta\tilde{u}_i\delta\tilde{u}_j+2\nu\frac{\partial^2}{\partial r_k\partial r_k}\delta\tilde{u}_i\delta\tilde{u}_j-\nu\frac{\partial\delta\tilde{u}_i}{\partial X_k}\frac{\partial\delta\tilde{u}_j}{\partial X_k}-4\nu\frac{\partial\delta\tilde{u}_i}{\partial r_k}\frac{\partial\delta\tilde{u}_j}{\partial r_k}\\
&\quad=\frac{\nu}{2}\frac{\partial^2}{\partial X_k\partial X_k}\delta\tilde{u}_i\delta\tilde{u}_j+2\nu\frac{\partial^2}{\partial r_k\partial r_k}\delta\tilde{u}_i\delta\tilde{u}_j-2\left(\epsilon_{ij}^{c+}+\epsilon_{ij}^{c}\right),
\end{aligned}\tag{A21}$$

where ϵ_{ij}^c is the pseudo-dissipation tensor of the coherent part of the velocity, defined as

$$\epsilon_{ij}^c=\nu\left\langle\frac{\partial\tilde{u}_i}{\partial x_k}\frac{\partial\tilde{u}_j}{\partial x_k}\right\rangle.\tag{A22}$$

Moreover we write

$$\delta\tilde{u}_j\delta\tilde{u}_k\frac{\partial\delta U_i}{\partial r_k}=\delta\tilde{u}_j\delta\tilde{u}_k\left(\frac{\partial U_i}{\partial x_k}\right)^*\tag{A23}$$

and

$$\delta\tilde{u}_j\tilde{u}_k^*\frac{\partial}{\partial X_k}\delta U_i=\delta\tilde{u}_j\tilde{u}_k^*\delta\left(\frac{\partial U_i}{\partial x_k}\right).\tag{A24}$$

Finally, the budget equation for $\delta\tilde{u}_i\delta\tilde{u}_j$ is obtained:

$$\begin{aligned}
&\frac{\partial}{\partial t}\delta\tilde{u}_i\delta\tilde{u}_j+\frac{\partial}{\partial r_k}\delta U_k\delta\tilde{u}_i\delta\tilde{u}_j+\frac{\partial}{\partial X_k}U_k^*\delta\tilde{u}_i\delta\tilde{u}_j+\frac{\partial}{\partial r_k}\delta\tilde{u}_k\delta\tilde{u}_i\delta\tilde{u}_j+\frac{\partial}{\partial X_k}\tilde{u}_k^*\delta\tilde{u}_i\delta\tilde{u}_j\\
&\quad+\frac{\partial}{\partial r_k}\overline{\delta u_k''\delta u_i''}\delta\tilde{u}_j+\frac{\partial}{\partial X_k}\overline{u_k''^{*}\delta u_i''}\delta\tilde{u}_j+\frac{\partial}{\partial r_k}\overline{\delta u_k''\delta u_j''}\delta\tilde{u}_i+\frac{\partial}{\partial X_k}\overline{u_k''^{*}\delta u_j''}\delta\tilde{u}_i\\
&\quad-2\nu\frac{\partial^2}{\partial r_k\partial r_k}\delta\tilde{u}_i\delta\tilde{u}_j-\frac{\nu}{2}\frac{\partial}{\partial X_k}\left(\frac{\partial}{\partial X_k}\delta\tilde{u}_i\delta\tilde{u}_j\right)+\frac{\partial}{\partial X_i}\frac{1}{\rho}\delta\tilde{p}\delta\tilde{u}_j+\frac{\partial}{\partial X_j}\frac{1}{\rho}\delta\tilde{p}\delta\tilde{u}_i\\
&\quad-\frac{\partial}{\partial r_k}\left\langle\delta\tilde{u}_i\delta\tilde{u}_k\right\rangle\delta\tilde{u}_j-\frac{\partial}{\partial X_k}\left\langle\tilde{u}_k^*\delta\tilde{u}_i\right\rangle\delta\tilde{u}_j-\frac{\partial}{\partial r_k}\left\langle\delta\tilde{u}_j\delta\tilde{u}_k\right\rangle\delta\tilde{u}_i-\frac{\partial}{\partial X_k}\left\langle\tilde{u}_k^*\delta\tilde{u}_j\right\rangle\delta\tilde{u}_i\\
&\quad-\frac{\partial}{\partial r_k}\left\langle\delta u_i''\delta u_k''\right\rangle\delta\tilde{u}_j-\frac{\partial}{\partial X_k}\left\langle u_k''^{*}\delta u_i''\right\rangle\delta\tilde{u}_j-\frac{\partial}{\partial r_k}\left\langle\delta u_j''\delta u_k''\right\rangle\delta\tilde{u}_i-\frac{\partial}{\partial X_k}\left\langle u_k''^{*}\delta u_j''\right\rangle\delta\tilde{u}_i
\end{aligned}$$

$$
\begin{aligned}
&= -\delta\tilde{u}_j\delta\tilde{u}_k\left(\frac{\partial U_i}{\partial x_k}\right)^* - \delta\tilde{u}_i\delta\tilde{u}_k\left(\frac{\partial U_j}{\partial x_k}\right)^* - \delta\tilde{u}_j\tilde{u}_k^*\delta\left(\frac{\partial U_i}{\partial x_k}\right) - \delta\tilde{u}_i\tilde{u}_k^*\delta\left(\frac{\partial U_j}{\partial x_k}\right)\\
&\quad - \langle\delta\tilde{u}_i\delta\tilde{u}_k\rangle\left(\frac{\partial\tilde{u}_j}{\partial x_k}\right)^* - \langle\delta\tilde{u}_j\delta\tilde{u}_k\rangle\left(\frac{\partial\tilde{u}_i}{\partial x_k}\right)^* - \langle\delta\tilde{u}_i\tilde{u}_k^*\rangle\delta\left(\frac{\partial\tilde{u}_j}{\partial x_k}\right) - \langle\delta\tilde{u}_j\tilde{u}_k^*\rangle\delta\left(\frac{\partial\tilde{u}_i}{\partial x_k}\right)\\
&\quad - \langle\delta u_i''\delta u_k''\rangle\left(\frac{\partial\tilde{u}_j}{\partial x_k}\right)^* - \langle\delta u_j''\delta u_k''\rangle\left(\frac{\partial\tilde{u}_i}{\partial x_k}\right)^* - \langle\delta u_i''u_k''^*\rangle\delta\left(\frac{\partial\tilde{u}_j}{\partial x_k}\right) - \langle\delta u_j''u_k''^*\rangle\delta\left(\frac{\partial\tilde{u}_i}{\partial x_k}\right)\\
&\quad + \overline{\delta u_i''\delta u_k''}\frac{\partial\delta\tilde{u}_j}{\partial r_k} + \overline{\delta u_i''u_k''^*}\frac{\partial\delta\tilde{u}_j}{\partial X_k} + \overline{\delta u_j''\delta u_k''}\frac{\partial\delta\tilde{u}_i}{\partial r_k} + \overline{\delta u_j''u_k''^*}\frac{\partial\delta\tilde{u}_i}{\partial X_k}\\
&\quad + \frac{1}{\rho}\delta\tilde{p}\frac{\partial\delta\tilde{u}_j}{\partial X_i} + \frac{1}{\rho}\delta\tilde{p}\frac{\partial\delta\tilde{u}_i}{\partial X_j} - 4\epsilon_{ij}^{c*} + \delta\tilde{u}_j\delta\tilde{f}_i + \delta\tilde{u}_i\delta\tilde{f}_j. \qquad \text{(A25)}
\end{aligned}
$$

A.3. *The φAGKE for* $\overline{\delta u_i''\delta u_j''}$

We write the budget equation for u_i'' twice for the positions $\boldsymbol{x}$ and $\boldsymbol{x}^+ = \boldsymbol{x} + \boldsymbol{r}$, then the first is subtracted from the second:

$$
\begin{aligned}
&\delta\left(\frac{\partial u_i''}{\partial t}\right) + \delta\left(U_k\frac{\partial u_i''}{\partial x_k}\right) + \delta\left(\tilde{u}_k\frac{\partial u_i''}{\partial x_k}\right) + \delta\left(u_k''\frac{\partial U_i}{\partial x_k}\right) + \delta\left(u_k''\frac{\partial\tilde{u}_i}{\partial x_k}\right)\\
&\quad + \delta\left(\frac{\partial}{\partial x_k}\left(u_i''u_k'' - \overline{u_i''u_k''}\right)\right) = -\delta\left(\frac{1}{\rho}\frac{\partial p''}{\partial x_i}\right) + \delta\left(\nu\frac{\partial^2 u_i''}{\partial x_k\partial x_k}\right) + \delta\left(f_i''\right). \qquad \text{(A26)}
\end{aligned}
$$

Following the line of reasoning described above, the equation for $\delta u_i''$ is obtained, i.e.

$$
\begin{aligned}
&\frac{\partial\delta u_i''}{\partial t} + \delta U_k\frac{\partial\delta u_i''}{\partial x_k^+} + U_k\frac{\partial\delta u_i''}{\partial x_k^+} + U_k\frac{\partial\delta u_i''}{\partial x_k} + \delta\tilde{u}_k\frac{\partial\delta u_i''}{\partial x_k^+} + \tilde{u}_k\frac{\partial\delta u_i''}{\partial x_k^+} + \tilde{u}_k\frac{\partial\delta u_i''}{\partial x_k}\\
&\quad + \delta u_k''\frac{\partial\delta U_i}{\partial x_k^+} + u_k''\frac{\partial\delta U_i}{\partial x_k^+} + u_k''\frac{\partial\delta U_i}{\partial x_k} + \delta u_k''\frac{\partial\delta\tilde{u}_i}{\partial x_k^+} + u_k''\frac{\partial\delta\tilde{u}_i}{\partial x_k^+} + u_k''\frac{\partial\delta\tilde{u}_i}{\partial x_k} + \delta u_k''\frac{\partial\delta u_i''}{\partial x_k^+}\\
&\quad + u_k''\frac{\partial\delta u_i''}{\partial x_k^+} + u_k''\frac{\partial\delta u_i''}{\partial x_k} - \overline{\delta u_k''\frac{\partial\delta u_i''}{\partial x_k^+}} - \overline{u_k''\left(\frac{\partial}{\partial x_k^+} + \frac{\partial}{\partial x_k}\right)\delta u_i''}\\
&= -\frac{1}{\rho}\frac{\partial\delta p''}{\partial x_i^+} - \frac{1}{\rho}\frac{\partial\delta p''}{\partial x_i} + \nu\left(\frac{\partial^2}{\partial x_k^+\partial x_k^+} + \frac{\partial^2}{\partial x_k\partial x_k}\right)\delta u_i + \delta f_i''. \qquad \text{(A27)}
\end{aligned}
$$

As above, we first multiply this equation for $\delta u_j''$, and then we sum to the same equation with swapped i and j indices. Using again the independence of the $\boldsymbol{x}$ and $\boldsymbol{x}^+$ reference systems and incompressibility, and applying the phase average operator $\overline{\cdot}$, we obtain

$$
\begin{aligned}
&\frac{\partial}{\partial t}\overline{\delta u_i''\delta u_j''} + \frac{\partial}{\partial x_k^+}\delta U_k\overline{\delta u_i''\delta u_j''} + \left(\frac{\partial}{\partial x_k^+} + \frac{\partial}{\partial x_k}\right)U_k\overline{\delta u_i''\delta u_j''} + \overline{\delta u_j''\delta u_k''}\frac{\partial\delta U_i}{\partial x_k^+} + \overline{\delta u_i''\delta u_k''}\frac{\partial\delta U_j}{\partial x_k^+}\\
&\quad + \overline{\delta u_j''u_k''}\left(\frac{\partial}{\partial x_k^+} + \frac{\partial}{\partial x_k}\right)\delta U_i + \overline{\delta u_i''u_k''}\left(\frac{\partial}{\partial x_k^+} + \frac{\partial}{\partial x_k}\right)\delta U_j + \frac{\partial}{\partial x_k^+}\delta\tilde{u}_k\overline{\delta u_j''\delta u_i''}
\end{aligned}
$$

$$
\begin{aligned}
&+\left(\frac{\partial}{\partial x_k^+}+\frac{\partial}{\partial x_k}\right)\tilde{u}_k\overline{\delta u_j''\delta u_i''}+\overline{\delta u_j''\delta u_k''}\frac{\partial\delta\tilde{u}_i}{\partial x_k^+}+\overline{\delta u_i''\delta u_k''}\frac{\partial\delta\tilde{u}_j}{\partial x_k^+}\\
&+\overline{\delta u_j''u_k''}\left(\frac{\partial}{\partial x_k^+}+\frac{\partial}{\partial x_k}\right)\delta\tilde{u}_i+\overline{\delta u_i''u_k''}\left(\frac{\partial}{\partial x_k^+}+\frac{\partial}{\partial x_k}\right)\delta\tilde{u}_j\\
&+\frac{\partial}{\partial x_k^+}\overline{\delta u_k''\delta u_i''\delta u_j''}+\left(\frac{\partial}{\partial x_k^+}+\frac{\partial}{\partial x_k}\right)\overline{u_k''\delta u_i''\delta u_j''}\\
=&-\frac{1}{\rho}\left(\frac{\partial}{\partial x_i^+}+\frac{\partial}{\partial x_i}\right)\overline{\delta p''\delta u_j''}-\frac{1}{\rho}\left(\frac{\partial}{\partial x_j^+}+\frac{\partial}{\partial x_j}\right)\overline{\delta p''\delta u_i''}\\
&+\overline{\frac{1}{\rho}\delta p''\left(\frac{\partial}{\partial x_i^+}+\frac{\partial}{\partial x_i}\right)\delta u_j''}+\overline{\frac{1}{\rho}\delta p''\left(\frac{\partial}{\partial x_j^+}+\frac{\partial}{\partial x_j}\right)\delta u_i''}\\
&+\overline{\nu\delta u_j''\left(\frac{\partial^2}{\partial x_k^+\partial x_k^+}+\frac{\partial^2}{\partial x_k\partial x_k}\right)\delta u_i''}+\overline{\nu\delta u_i''\left(\frac{\partial^2}{\partial x_k^+\partial x_k^+}+\frac{\partial^2}{\partial x_k\partial x_k}\right)\delta u_j''}\\
&+\overline{\delta f_i''\delta u_j''}+\overline{\delta f_j''\delta u_i''}.
\end{aligned}
\tag{A28}
$$

We switch as above to the notation with $\boldsymbol{X}$ and $\boldsymbol{r}$ to obtain

$$
\begin{aligned}
&\frac{\partial}{\partial t}\overline{\delta u_i''\delta u_j''}+\frac{\partial}{\partial r_k}U_k\overline{\delta\delta u_i''\delta u_j''}+\frac{\partial}{\partial X_k}U_k^*\overline{\delta u_i''\delta u_j''}+\overline{\delta u_j''\delta u_k''}\frac{\partial\delta U_i}{\partial r_k}+\overline{\delta u_i''\delta u_k''}\frac{\partial\delta U_j}{\partial r_k}\\
&+\overline{\delta u_j''u_k''^*}\frac{\partial\delta U_i}{\partial X_k}+\overline{\delta u_i''u_k''^*}\frac{\partial\delta U_j}{\partial X_k}+\overline{\delta u_j''\delta u_k''}\frac{\partial\delta\tilde{u}_i}{\partial r_k}+\overline{\delta u_j''u_k''^*}\frac{\partial\delta\tilde{u}_i}{\partial X_k}+\overline{\delta u_i''\delta u_k''}\frac{\partial\delta\tilde{u}_j}{\partial r_k}\\
&+\overline{\delta u_j''u_k''^*}\frac{\partial\delta\tilde{u}_j}{\partial X_k}+\frac{\partial}{\partial r_k}\overline{\delta u_k''\delta u_i''\delta u_j''}+\frac{\partial}{\partial X_k}\overline{u_k''^*\delta u_i''\delta u_j''}+\frac{\partial}{\partial r_k}\delta\tilde{u}_k\overline{\delta u_i''\delta u_j''}\\
&+\frac{\partial}{\partial X_k}\tilde{u}_k^*\overline{\delta u_i''\delta u_j''}+\frac{\partial}{\partial X_i}\frac{1}{\rho}\overline{\delta p''\delta u_j''}+\frac{\partial}{\partial X_j}\frac{1}{\rho}\overline{\delta p''\delta u_i''}=\frac{1}{\rho}\overline{\delta p''\frac{\partial\delta u_j''}{\partial X_i}}+\frac{1}{\rho}\overline{\delta p''\frac{\partial\delta u_i''}{\partial X_j}}\\
&+\frac{\nu}{2}\frac{\partial^2}{\partial X_k\partial X_k}\overline{\delta u_i''\delta u_j''}+2\nu\frac{\partial^2}{\partial r_k\partial r_k}\overline{\delta u_i''\delta u_j''}-2\left(\epsilon_{ij}^{s+}+\epsilon_{ij}^{s}\right)+\overline{\delta f_i''\delta u_j''}+\overline{\delta f_j''\delta u_i''},
\end{aligned}
\tag{A29}
$$

where

$$
\epsilon_{ij}^{s}=\nu\overline{\frac{\partial u_i''}{\partial x_k}\frac{\partial u_j''}{\partial x_k}}
\tag{A30}
$$

is the pseudo-dissipation tensor of the stochastic part of the velocity. Also in this case we can write

$$
\overline{\delta u_j''\delta u_k''}\frac{\partial\delta U_i}{\partial r_k}=\overline{\delta u_j''\delta u_k''}\left(\frac{\partial U_i}{\partial x_k}\right)^*
\tag{A31}
$$

and

$$
\overline{\delta u_j''u_k''^*}\frac{\partial\delta U_i}{\partial X_k}=\overline{\delta u_j''u_k''^*}\delta\left(\frac{\partial U_i}{\partial x_k}\right)
\tag{A32}
$$

so that the budget equation for $\overline{\delta u_i'' \delta u_j''}$ is eventually obtained:

$$\begin{aligned}
&\frac{\partial}{\partial t}\overline{\delta u_i'' \delta u_j''} + \frac{\partial}{\partial r_k}\delta U_k \overline{\delta u_i'' \delta u_j''} + \frac{\partial}{\partial X_k} U_k^* \overline{\delta u_i'' \delta u_j''} + \frac{\partial}{\partial r_k}\overline{\delta u_k'' \delta u_i'' \delta u_j''} + \frac{\partial}{\partial X_k}\overline{u_k''^* \delta u_i'' \delta u_j''} \\
&\quad + \frac{\partial}{\partial r_k}\left(-2\nu \frac{\partial}{\partial r_k}\overline{\delta u_i'' \delta u_j''}\right) + \frac{\partial}{\partial X_k}\left(-\frac{\nu}{2}\frac{\partial}{\partial X_k}\overline{\delta u_i'' \delta u_j''}\right) + \frac{\partial}{\partial r_k}\delta \tilde{u}_k \overline{\delta u_i'' \delta u_j''} + \frac{\partial}{\partial X_k}\tilde{u}_k^* \overline{\delta u_i'' \delta u_j''} \\
&\quad + \frac{\partial}{\partial X_i}\frac{1}{\rho}\overline{\delta p'' \delta u_j''} + \frac{\partial}{\partial X_j}\frac{1}{\rho}\overline{\delta p'' \delta u_i''} = -\overline{\delta u_j'' \delta u_k''}\left(\frac{\partial U_i}{\partial x_k}\right)^* - \overline{\delta u_i'' \delta u_k''}\left(\frac{\partial U_j}{\partial X_k}\right)^* \\
&\quad - \overline{\delta u_j'' u_k''^*}\delta\left(\frac{\partial U_i}{\partial x_k}\right) - \overline{\delta u_i'' u_k''^*}\delta\left(\frac{\partial U_j}{\partial x_k}\right) - \overline{\delta u_j'' \delta u_k''}\left(\frac{\partial \tilde{u}_i}{\partial x_k}\right)^* - \overline{\delta u_i'' \delta u_k''}\left(\frac{\partial \tilde{u}_j}{\partial x_k}\right)^* \\
&\quad - \overline{\delta u_j'' u_k''^*}\delta\left(\frac{\partial \tilde{u}_i}{\partial x_k}\right) - \overline{\delta u_i'' u_k''^*}\delta\left(\frac{\partial \tilde{u}_j}{\partial x_k}\right) + \frac{1}{\rho}\overline{\delta p''\frac{\partial \delta u_j''}{\partial X_i}} + \frac{1}{\rho}\overline{\delta p''\frac{\partial \delta u_i''}{\partial X_j}} \\
&\quad - 4\epsilon_{ij}^{s*} + \overline{\delta f_i'' \delta u_j''} + \overline{\delta f_j'' \delta u_i''}.
\end{aligned} \tag{A33}$$

Appendix B. The φAGKE for plane channel flow with oscillating walls

The special form assumed by the φAGKE under the symmetries of a plane channel flow with spanwise oscillations is reported below. The coherent part reduces to

$$\begin{aligned}
&\omega\frac{\partial \delta\tilde{u}_i \delta\tilde{u}_j}{\partial \varphi} + \frac{\partial}{\partial r_k}\underbrace{\left(\overline{\delta u_k'' \delta u_i''}\delta\tilde{u}_j + \overline{\delta u_k'' \delta u_j''}\delta\tilde{u}_i\right)}_{\text{Turbulent transport}} + \frac{\partial}{\partial r_y}\underbrace{\left(-2\nu\frac{\partial \delta\tilde{u}_i\delta\tilde{u}_j}{\partial r_y}\right)}_{\text{Viscous diffusion}} + \frac{\partial}{\partial Y}\underbrace{\left(-\frac{\nu}{2}\frac{\partial \delta\tilde{u}_i\delta\tilde{u}_j}{\partial Y}\right)}_{\text{Viscous diffusion}} \\
&\quad + \frac{\partial}{\partial Y}\underbrace{\left(\overline{v''^* \delta u_i''}\delta\tilde{u}_j + \overline{v''^* \delta u_j''}\delta\tilde{u}_i\right)}_{\text{Turbulent transport}} + \frac{\partial}{\partial Y}\underbrace{\left(\frac{1}{\rho}\delta\tilde{p}\delta\tilde{u}_i\delta_{j2}\right)}_{\text{Pressure transport}} + \frac{\partial}{\partial Y}\underbrace{\left(\frac{1}{\rho}\delta\tilde{p}\delta\tilde{u}_j\delta_{i2}\right)}_{\text{Pressure transport}} \\
&= -\underbrace{\begin{bmatrix} -\overline{\delta u_i'' \delta v''}\left(\frac{\partial \tilde{u}}{\partial y}\right)^*\delta_{j1} - \overline{\delta u_j'' \delta v''}\left(\frac{\partial \tilde{u}}{\partial y}\right)^*\delta_{i1} \\ -\overline{\delta u_i'' v''^*}\delta\left(\frac{\partial \tilde{u}}{\partial y}\right)\delta_{j1} - \overline{\delta u_j'' v''^*}\delta\left(\frac{\partial \tilde{u}}{\partial y}\right)\delta_{i1} \end{bmatrix}}_{p_{ij}^{cs}} \\
&\quad - \underbrace{\begin{bmatrix} -\overline{\delta u_i'' \delta v''}\left(\frac{\partial \tilde{w}}{\partial y}\right)^*\delta_{j3} - \overline{\delta u_j'' \delta v''}\left(\frac{\partial \tilde{w}}{\partial y}\right)^*\delta_{i3} \\ -\overline{\delta u_i'' v''^*}\delta\left(\frac{\partial \tilde{w}}{\partial y}\right)\delta_{j3} - \overline{\delta u_j'' v''^*}\delta\left(\frac{\partial \tilde{w}}{\partial y}\right)\delta_{i3} \end{bmatrix}}_{p_{ij}^{cs}} \\
&\quad + \underbrace{\frac{1}{\rho}\delta\tilde{p}\frac{\partial \delta\tilde{u}_i}{\partial Y}\delta_{j2} + \frac{1}{\rho}\delta\tilde{p}\frac{\partial \delta\tilde{u}_j}{\partial Y}\delta_{i2}}_{\pi_{ij}^c} \underbrace{- 4\epsilon_{ij}^{c*}}_{d_{ij}^c}
\end{aligned}$$

$$+\underbrace{\frac{\partial}{\partial r_k}\left[\left\langle\delta u_i''\delta u_k''\right\rangle\delta\tilde{u}_j+\left\langle\delta u_j''\delta u_k''\right\rangle\delta\tilde{u}_i\right]+\frac{\partial}{\partial Y}\left[\left\langle v''^{*}\delta u_i''\right\rangle\delta\tilde{u}_j+\left\langle v''^{*}\delta u_j''\right\rangle\delta\tilde{u}_i\right]}_{\zeta_{ij}^{c}}$$

$$+\underbrace{\left[-\left\langle\delta u_i''\delta v''\right\rangle\left(\frac{\partial\tilde{u}_j}{\partial y}\right)^{*}-\left\langle\delta u_j''\delta v''\right\rangle\left(\frac{\partial\tilde{u}_i}{\partial y}\right)^{*}-\left\langle\delta u_i''v''^{*}\right\rangle\delta\left(\frac{\partial\tilde{u}_j}{\partial y}\right)-\left\langle\delta u_j''v''^{*}\right\rangle\delta\left(\frac{\partial\tilde{u}_i}{\partial y}\right)\right]}_{\zeta_{ij}^{c}}. \tag{B1}$$

The φAGKE for the stochastic part $\overline{\delta u_i''\delta u_j''}$ become

$$\omega\frac{\partial\overline{\delta u_i''\delta u_j''}}{\partial\varphi}+\frac{\partial}{\partial r_x}\underbrace{\left(\delta U\overline{\delta u_i''\delta u_j''}\right)}_{\text{Mean transport}}+\frac{\partial}{\partial r_x}\underbrace{\left(\delta\tilde{u}\overline{\delta u_i''\delta u_j''}\right)}_{\text{Coherent transport}}+\frac{\partial}{\partial r_z}\underbrace{\left(\delta\tilde{w}\overline{\delta u_i''\delta u_j''}\right)}_{\text{Coherent transport}}$$

$$+\frac{\partial}{\partial r_k}\underbrace{\left(\overline{\delta u_k''\delta u_i''\delta u_j''}\right)}_{\text{Turbulent transport}}+\frac{\partial}{\partial r_k}\underbrace{\left(-2\nu\frac{\partial\overline{\delta u_i''\delta u_j''}}{\partial r_k}\right)}_{\text{Viscous diffusion}}+\frac{\partial}{\partial Y}\underbrace{\left(\overline{v''^{*}\delta u_i''\delta u_j''}\right)}_{\text{Turbulent transport}}$$

$$+\frac{\partial}{\partial Y}\underbrace{\left(-\frac{\nu}{2}\frac{\partial\overline{\delta u_i''\delta u_j''}}{\partial Y}\right)}_{\text{Viscous diffusion}}+\frac{\partial}{\partial Y}\underbrace{\left(\frac{1}{\rho}\overline{\delta p''\delta u_j''}\delta_{i2}+\frac{1}{\rho}\overline{\delta p''\delta u_i''}\delta_{j2}\right)}_{\text{Pressure transport}}$$

$$=\underbrace{\begin{bmatrix}-\overline{\delta u_i''\delta v''}\left(\frac{\mathrm{d}U}{\mathrm{d}y}\right)^{*}\delta_{j1}-\overline{\delta u_j''\delta v''}\left(\frac{\mathrm{d}U}{\mathrm{d}y}\right)^{*}\delta_{i1}\\ -\overline{\delta u_i''v''^{*}}\delta\left(\frac{\mathrm{d}U}{\mathrm{d}y}\right)\delta_{j1}-\overline{\delta u_j''v''^{*}}\delta\left(\frac{\mathrm{d}U}{\mathrm{d}y}\right)\delta_{i1}\end{bmatrix}}_{p_{ij}^{ms}}$$

$$+\underbrace{\begin{bmatrix}-\overline{\delta u_i''\delta v''}\left(\frac{\partial\tilde{u}}{\partial y}\right)^{*}\delta_{j1}-\overline{\delta u_j''\delta v''}\left(\frac{\partial\tilde{u}}{\partial y}\right)^{*}\delta_{i1}\\ -\overline{\delta u_i''v''^{*}}\delta\left(\frac{\partial\tilde{u}}{\partial y}\right)\delta_{j1}-\overline{\delta u_j''v''^{*}}\delta\left(\frac{\partial\tilde{u}}{\partial y}\right)\delta_{i1}\end{bmatrix}}_{p_{ij}^{cs}}$$

$$+\underbrace{\begin{bmatrix}-\overline{\delta u_i''\delta v''}\left(\frac{\partial\tilde{w}}{\partial y}\right)^{*}\delta_{j3}-\overline{\delta u_j''\delta v''}\left(\frac{\partial\tilde{w}}{\partial y}\right)^{*}\delta_{i3}\\ -\overline{\delta u_i''v''^{*}}\delta\left(\frac{\partial\tilde{w}}{\partial y}\right)\delta_{j3}-\overline{\delta u_j''v''^{*}}\delta\left(\frac{\partial\tilde{w}}{\partial y}\right)\delta_{i3}\end{bmatrix}}_{p_{ij}^{cs}}$$

$$\underbrace{+\frac{1}{\rho}\overline{\delta p''\left(\frac{\partial\delta u_i''}{\partial X_j}\right)}+\frac{1}{\rho}\overline{\delta p''\left(\frac{\partial\delta u_j''}{\partial X_i}\right)}}_{\pi_{ij}^{s}}\underbrace{-4\epsilon_{ij}^{s*}}_{d_{ij}^{s}}. \tag{B2}$$

Here, the mean transport term contributes to ϕ_x^s, consistently with a non-zero streamwise mean velocity U. Similarly, coherent transport appears in ϕ_x^s and ϕ_z^s, since $\tilde{u} \neq 0$ and $\tilde{w} \neq 0$. Since no external volume forcing acts on the flow, the interaction forcing term is zero for both components.

Appendix C. Analysis of conditionally averaged quantities

In this appendix, the interpretations of the local maxima of $\overline{\delta w'' \delta w''}$ in the $r_x = r_y = 0$ and $r_z = r_y = 0$ planes provided in § 4.1.2 are supported by inspecting the velocity field induced by the conditionally averaged quasi-streamwise vortex at different phases of the control cycle. The procedure to extract the conditional average from the direct numerical simulation database closely resembles that presented by Jeong *et al.* (1997); it is described in detail by Gallorini *et al.* (2022) and is not repeated here.

Figure 15 uses velocity isosurfaces to describe the spatial shape of the conditionally averaged negative rotating (SN) structure for the case at $T^+ = 250$ at the two phases φ_1 and φ_3. The extraction procedure is centred at the wall-normal position of the maxima of $\overline{\delta w'' \delta w''}$ for φ_1 and φ_3 (see figure 4): this position is shown in the shear panel at the bottom of figure 15. At the two chosen phases, the structures show their maximum negative and positive tilt angle; however, the discussion below for φ_1 can be extended to φ_2, and that for φ_3 extends to φ_4. Isocontours of streamwise (transparent) and spanwise (solid colour) velocities are shown in a view from above (top) and from upstream (bottom).

Following the discussion in § 4.1.2, when the tilting angle is negative (see φ_1), the low-speed streak associated with a SN structure redistributes its energy via pressure strain and creates negative spanwise velocity fluctuations; the opposite occurs for the high-speed streak. This is confirmed by the ensemble-averaged structure, which shows a region of positive (negative) spanwise velocity close to the side of the high-speed (low-speed) streak. At φ_3, instead, the tilt angle of the streak is positive, and the low-speed (high-speed) streak induces positive (negative) w'' velocity fluctuations at its side.

Another view of the spanwise velocity contours is displayed in figure 15(*c*,*d*). In these images, the streamwise velocity contours are removed, to focus on the spanwise component only. In the canonical channel flow, a negatively rotating vortex induces two regions of high and low spanwise velocity below and above its centre, respectively. However, when the wall oscillates, two additional regions of positive and negative spanwise velocity originate at the sides of the tilted vortex because of its interaction with the Stokes layer. At phase φ_1 (figure 15*c*), the peak of $\overline{\delta w'' \delta w''}$ occurs at $Y^+ = 25$, where the spanwise shear $\partial \tilde{w}^+ / \partial y$ is positive. Therefore, the negatively rotating quasi-streamwise vortex lifts low spanwise velocity fluid, and displaces high-spanwise-velocity fluid downwards. This process explains the appearance of a low w-velocity region at the right-hand side of the quasi-streamwise vortex, whereas the high-spanwise-velocity region is absorbed into the lower-side one. At φ_3 the regions of low/high spanwise velocity are opposite compared with φ_1 owing to the opposite sign of the spanwise shear at the location of the peak of $\overline{\delta w'' \delta w''}$ at this phase.

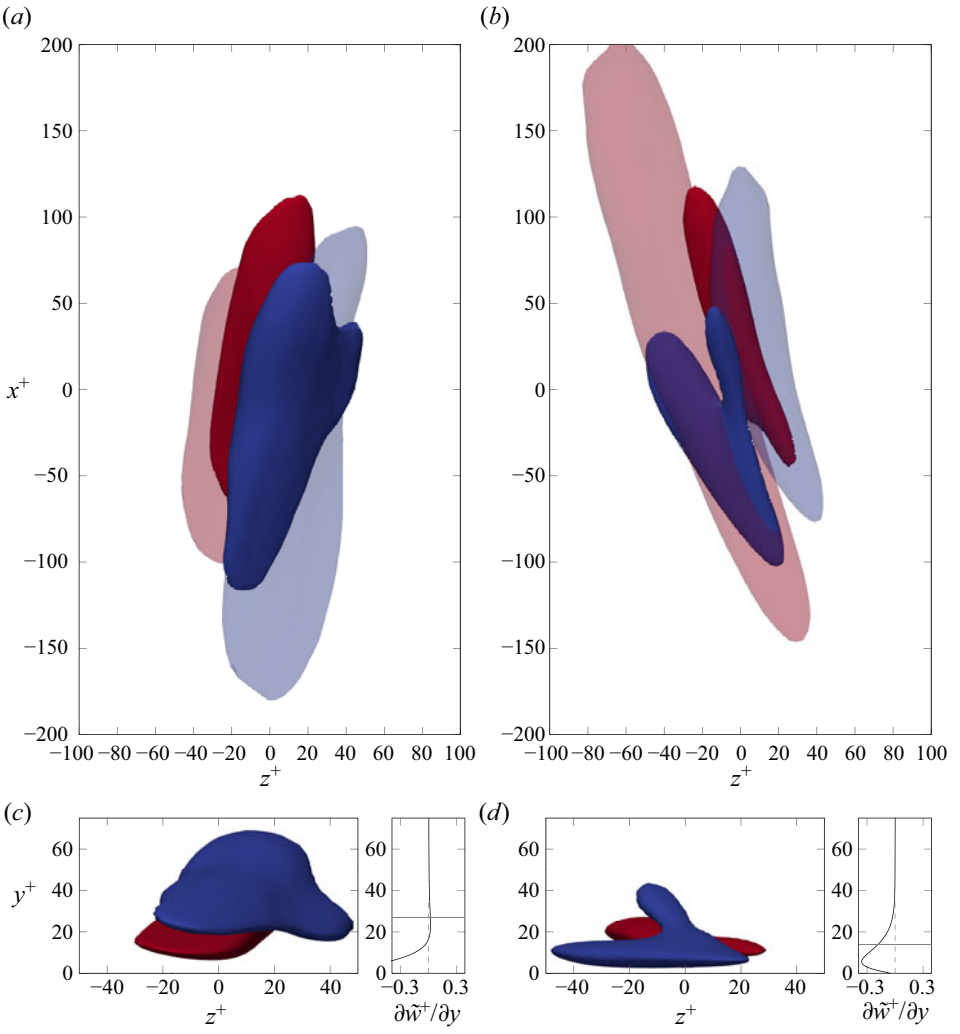

Figure 15. Conditionally averaged structure, extracted at φ_1 (*a*,*c*) and φ_3 (*b*,*d*) at $T^+ = 250$. The spatial shape of the structure is shown via isosurfaces of u'^+ (transparent colour) and w'^+ (solid colour) velocity fluctuations at the level ± 0.5 (red/blue is positive/negative). The bottom panels also include the spanwise shear $\mathrm{d}\tilde{w}^+/\mathrm{d}y$ at that phase, and show the wall-normal position where the extraction procedure is carried out.

References

Agostini, L. & Leschziner, M.A. 2014 On the influence of outer large-scale structures on near-wall turbulence in channel flow. *Phys. Fluids* **26** (7), 075107.

Agostini, L. & Leschziner, M. 2017 Spectral analysis of near-wall turbulence in channel flow at $Re_\tau = 4200$ with emphasis on the attached-eddy hypothesis. *Phys. Rev. Fluids* **2** (1), 014603.

Agostini, L., Touber, E. & Leschziner, M.A. 2014 Spanwise oscillatory wall motion in channel flow: drag-reduction mechanisms inferred from DNS-predicted phase-wise property variations at $Re_\tau = 1000$. *J. Fluid Mech.* **743**, 606–635.

Alves Portela, F., Papadakis, G. & Vassilicos, J.C. 2017 The turbulence cascade in the near wake of a square prism. *J. Fluid Mech.* **825**, 315–352.

Alves Portela, F., Papadakis, G. & Vassilicos, J.C. 2020 The role of coherent structures and inhomogeneity in near-field interscale turbulent energy transfers. *J. Fluid Mech.* **896**, A16–A24.

Andreolli, A., Quadrio, M. & Gatti, D. 2021 Global energy budgets in turbulent Couette and Poiseuille flows. *J. Fluid Mech.* **924**, A25.

ARUN, S., SAMEEN, A., SRINIVASAN, B. & GIRIMAJI, S.S. 2021 Scale-space energy density function transport equation for compressible inhomogeneous turbulent flows. *J. Fluid Mech.* **920**, A31.

BARON, A. & QUADRIO, M. 1996 Turbulent drag reduction by spanwise wall oscillations. *Appl. Sci. Res.* **55**, 311–326.

BECH, K.H. & ANDERSSON, H.I. 1996 Secondary flow in weakly rotating turbulent plane Couette flow. *J. Fluid Mech.* **317**, 195–214.

CHIARINI, A., GATTI, D., CIMARELLI, A. & QUADRIO, M. 2022*a* Structure of turbulence in the flow around a rectangular cylinder. *J. Fluid Mech.* **946**, A35.

CHIARINI, A., MAURIELLO, M., GATTI, D. & QUADRIO, M. 2022*b* Ascending-descending and direct-inverse cascades of Reynolds stresses in turbulent Couette flow. *J. Fluid Mech.* **930**, A9–A22.

CIMARELLI, A., DE ANGELIS, E. & CASCIOLA, C.M. 2013 Paths of energy in turbulent channel flows. *J. Fluid Mech.* **715**, 436–451.

CIMARELLI, A., DE ANGELIS, E., JIMENEZ, J. & CASCIOLA, C.M. 2016 Cascades and wall-normal fluxes in turbulent channel flows. *J. Fluid Mech.* **796**, 417–436.

CIMARELLI, A., MOLLICONE, J.-P., VAN REEUWIJK, M. & DE ANGELIS, E. 2021 Spatially evolving cascades in temporal planar jets. *J. Fluid Mech.* **910**, A19–A31.

DANAILA, L., ANSELMET, F., ZHOU, T. & ANTONIA, R.A. 2001 Turbulent energy scale budget equations in a fully developed channel flow. *J. Fluid Mech.* **430**, 87–109.

DANAILA, L., VOIVENEL, L. & VAREA, E. 2017 Self-similarity criteria in anisotropic flows with viscosity stratification. *Phys. Fluids* **29** (2), 020716.

DAVIDSON, P.A., NICKELS, T.B. & KROGSTAD, P.-Å. 2006 The logarithmic structure function law in wall-layer turbulence. *J. Fluid Mech.* **550**, 51–60.

FROHNAPFEL, B., HASEGAWA, Y. & QUADRIO, M. 2012 Money versus time: evaluation of flow control in terms of energy consumption and convenience. *J. Fluid Mech.* **700**, 406–418.

GAI, J., XIA, Z., CAI, Q. & CHEN, S. 2016 Turbulent statistics and flow structures in spanwise-rotating turbulent plane Couette flows. *Phys. Rev. Fluids* **1** (5), 054401.

GALLORINI, E., QUADRIO, M. & GATTI, D. 2022 Coherent near-wall structures and drag reduction by spanwise forcing. *Phys. Rev. Fluids* **7** (11), 114602.

GATTI, D., CHIARINI, A., CIMARELLI, A. & QUADRIO, M. 2020 Structure function tensor equations in inhomogeneous turbulence. *J. Fluid Mech.* **898**, A5–A33.

GATTI, D. & QUADRIO, M. 2016 Reynolds-number dependence of turbulent skin-friction drag reduction induced by spanwise forcing. *J. Fluid Mech.* **802**, 553–558.

GATTI, D., REMIGI, A., CHIARINI, A., CIMARELLI, A. & QUADRIO, M. 2019 An efficient numerical method for the Generalized Kolmogorov Equation. *J. Turbul.* **20** (8), 457–480.

HILL, R.J. 2001 Equations relating structure functions of all orders. *J. Fluid Mech.* **434**, 379–388.

JEONG, J., HUSSAIN, F., SCHOPPA, W. & KIM, J. 1997 Coherent structures near the wall in a turbulent channel flow. *J. Fluid Mech.* **332**, 185–214.

JUNG, W.J., MANGIAVACCHI, N. & AKHAVAN, R. 1992 Suppression of turbulence in wall-bounded flows by high-frequency spanwise oscillations. *Phys. Fluids* A **4** (8), 1605–1607.

KAWATA, T. & ALFREDSSON, P.H. 2018 Inverse interscale transport of the Reynolds shear stress in plane Couette turbulence. *Phys. Rev. Lett.* **120** (24), 244501.

KIYA, M. & MATSUMURA, M. 1988 Incoherent turbulence structure in the near wake of a normal plate. *J. Fluid Mech.* **190**, 343–356.

KOSCHMIEDER, E.L. 1979 Turbulent Taylor vortex flow. *J. Fluid Mech.* **93**, 515–527.

LAI, C.K., CHARONKO, J.J. & PRESTRIDGE, K. 2018 A Kármán–Howarth–Monin equation for variable-density turbulence. *J. Fluid Mech.* **843**, 382–418.

LUCHINI, P. 2020 CPL. Available at https://CPLcode.net.

LUCHINI, P. 2021 Introducing CPL. arXiv:2012.12143.

MANSOUR, N., KIM, J. & MOIN, P. 1988 Reynolds-stress and dissipation-rate budgets in a turbulent channel flow. *J. Fluid Mech.* **194**, 15–44.

MOLLICONE, J.-P., BATTISTA, F., GUALTIERI, P. & CASCIOLA, C.M. 2018 Turbulence dynamics in separated flows: the generalised Kolmogorov equation for inhomogeneous anisotropic conditions. *J. Fluid Mech.* **841**, 1012–1039.

PROVANSAL, M., MATHIS, C. & BOYER, L. 1987 Bénard-von Kármán instability: transient and forced regimes. *J. Fluid Mech.* **182**, 1–22.

QUADRIO, M. 2011 Drag reduction in turbulent boundary layers by in-plane wall motion. *Phil. Trans. R. Soc.* A **369** (1940), 1428–1442.

QUADRIO, M., FROHNAPFEL, B. & HASEGAWA, Y. 2016 Does the choice of the forcing term affect flow statistics in DNS of turbulent channel flow? *Eur. J. Mech. (B/Fluids)* **55**, 286–293.

QUADRIO, M. & RICCO, P. 2004 Critical assessment of turbulent drag reduction through spanwise wall oscillation. *J. Fluid Mech.* **521**, 251–271.

QUADRIO, M. & RICCO, P. 2011 The laminar generalized Stokes layer and turbulent drag reduction. *J. Fluid Mech.* **667**, 135–157.

QUADRIO, M. & SIBILLA, S. 2000 Numerical simulation of turbulent flow in a pipe oscillating around its axis. *J. Fluid Mech.* **424**, 217–241.

RICCO, P., SKOTE, M. & LESCHZINER, M.A. 2021 A review of turbulent skin-friction drag reduction by near-wall transverse forcing. *Prog. Aerosp. Sci.* **123**, 100713.

THIESSET, F. & DANAILA, L. 2020 The illusion of a Kolmogorov cascade. *J. Fluid Mech.* **902**, F1.

THIESSET, F., DANAILA, L. & ANTONIA, R.A. 2014 Dynamical interactions between the coherent motion and small scales in a cylinder wake. *J. Fluid Mech.* **749**, 201–226.

TOUBER, E. & LESCHZINER, M.A. 2012 Near-wall streak modification by spanwise oscillatory wall motion and drag-reduction mechanisms. *J. Fluid Mech.* **693**, 150–200.

YAKENO, A., HASEGAWA, Y. & KASAGI, N. 2014 Modification of quasi-streamwise vortical structure in a drag-reduced turbulent channel flow with spanwise wall oscillation. *Phys. Fluids* **26**, 085109.

YAO, H., MOLLICONE, J.-P. & PAPADAKIS, G. 2022 Analysis of interscale energy transfer in a boundary layer undergoing bypass transition. *J. Fluid Mech.* **941**, A14.

YOUNG, G.S., KRISTOVICH, D.A.R., HJELMFELT, M.R. & FOSTER, R.C. 2002 Rolls, streets, waves and more: a review of quasi-two-dimensional structures in the atmospheric boundary layer. *Bull. Am. Meteorol. Soc.* **83** (7), 997–1002.